



# In Situ Generated Novel $^1\text{H}$ MRI Reporter for $\beta$ -Galactosidase Activity Detection and Visualization in Living Tumor Cells

Shuo Gao<sup>1</sup>, Lei Zhao<sup>1†</sup>, Zhiqiang Fan<sup>1†</sup>, Vikram D. Kodibagkar<sup>2</sup>, Li Liu<sup>3</sup>, Hanqin Wang<sup>1</sup>, Hong Xu<sup>1</sup>, Mingli Tu<sup>1</sup>, Bifu Hu<sup>1</sup>, Chuanbin Cao<sup>1</sup>, Zhenjian Zhang<sup>1</sup> and Jian-Xin Yu<sup>1,4\*</sup>

<sup>1</sup>Center of Translational Medicine, Fifth School of Medicine/Suizhou Central Hospital, Hubei University of Medicine, Suizhou, China, <sup>2</sup>School of Biological and Health Systems Engineering, Arizona State University, Tempe, AZ, United States, <sup>3</sup>Department of Radiology, University of Texas Southwestern Medical Center at Dallas, Dallas, TX, United States, <sup>4</sup>Biomedical Research Institute, Hubei University of Medicine, Shiyan, China

## OPEN ACCESS

### Edited by:

Jinwu Yan,  
South China University of Technology,  
China

### Reviewed by:

Chuqiao Tu,  
University of California, Davis,  
United States  
Wei Chen,  
University of Texas at Arlington,  
United States

### \*Correspondence:

Jian-Xin Yu  
jianxinyu707@gmail.com

<sup>†</sup>These authors have contributed  
equally to this work

### Specialty section:

This article was submitted to  
Chemical Biology,  
a section of the journal  
Frontiers in Chemistry

Received: 14 May 2021

Accepted: 16 June 2021

Published: 15 July 2021

### Citation:

Gao S, Zhao L, Fan Z, Kodibagkar VD,  
Liu L, Wang H, Xu H, Tu M, Hu B,  
Cao C, Zhang Z and Yu J-X (2021) In  
Situ Generated Novel  $^1\text{H}$  MRI Reporter  
for  $\beta$ -Galactosidase Activity Detection  
and Visualization in Living Tumor Cells.  
Front. Chem. 9:709581.  
doi: 10.3389/fchem.2021.709581

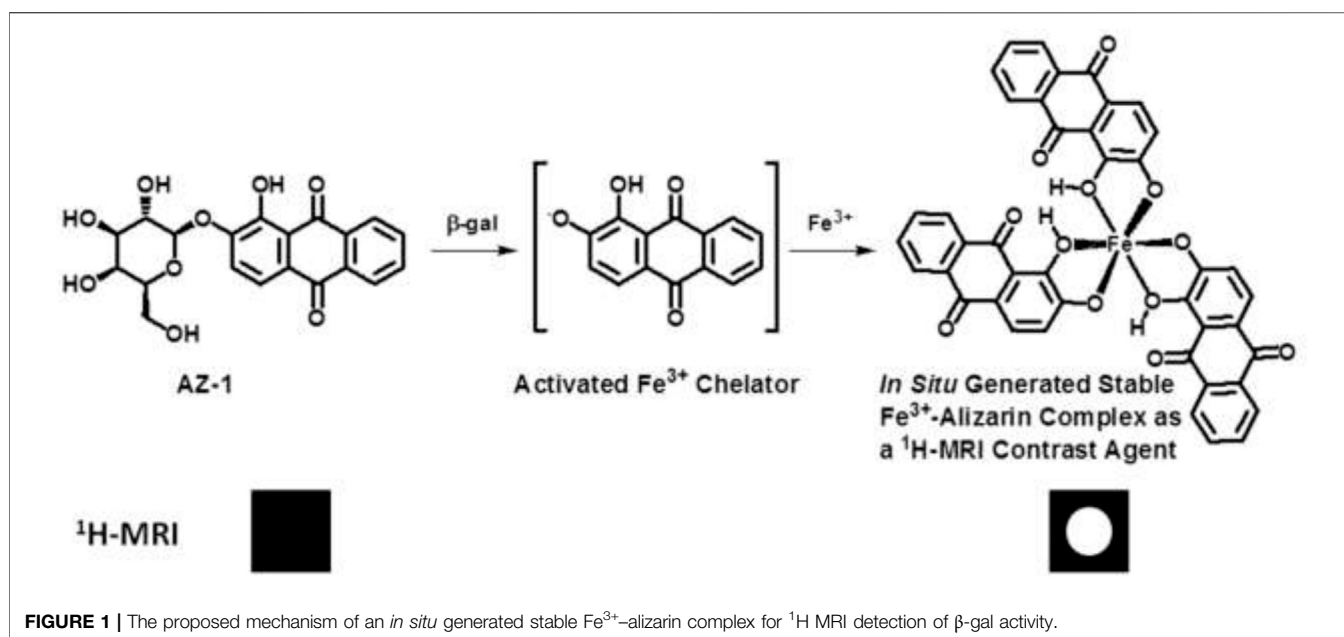
For wide applications of the *lacZ* gene in cellular/molecular biology, small animal investigations, and clinical assessments, the improvement of noninvasive imaging approaches to precisely assay gene expression has garnered much attention. In this study, we investigate a novel molecular platform in which alizarin 2-O- $\beta$ -D-galactopyranoside **AZ-1** acts as a *lacZ* gene/ $\beta$ -gal responsive  $^1\text{H}$ -MRI probe to induce significant  $^1\text{H}$ -MRI contrast changes in relaxation times  $T_1$  and  $T_2$  *in situ* as a concerted effect for the discovery of  $\beta$ -gal activity with the exposure of  $\text{Fe}^{3+}$ . We also demonstrate the capability of this strategy for detecting  $\beta$ -gal activity with *lacZ*-transfected human MCF7 breast and PC3 prostate cancer cells by reaction-enhanced  $^1\text{H}$ -MRI  $T_1$  and  $T_2$  relaxation mapping.

**Keywords:**  $\beta$ -galactosidase detection, responsive Fe-based  $^1\text{H}$ -MRI agent,  $T_1$  and  $T_2$  relaxation mapping, *in vitro*  $^1\text{H}$ -MRI imaging, *lacZ* gene reporter, synthesis

## INTRODUCTION

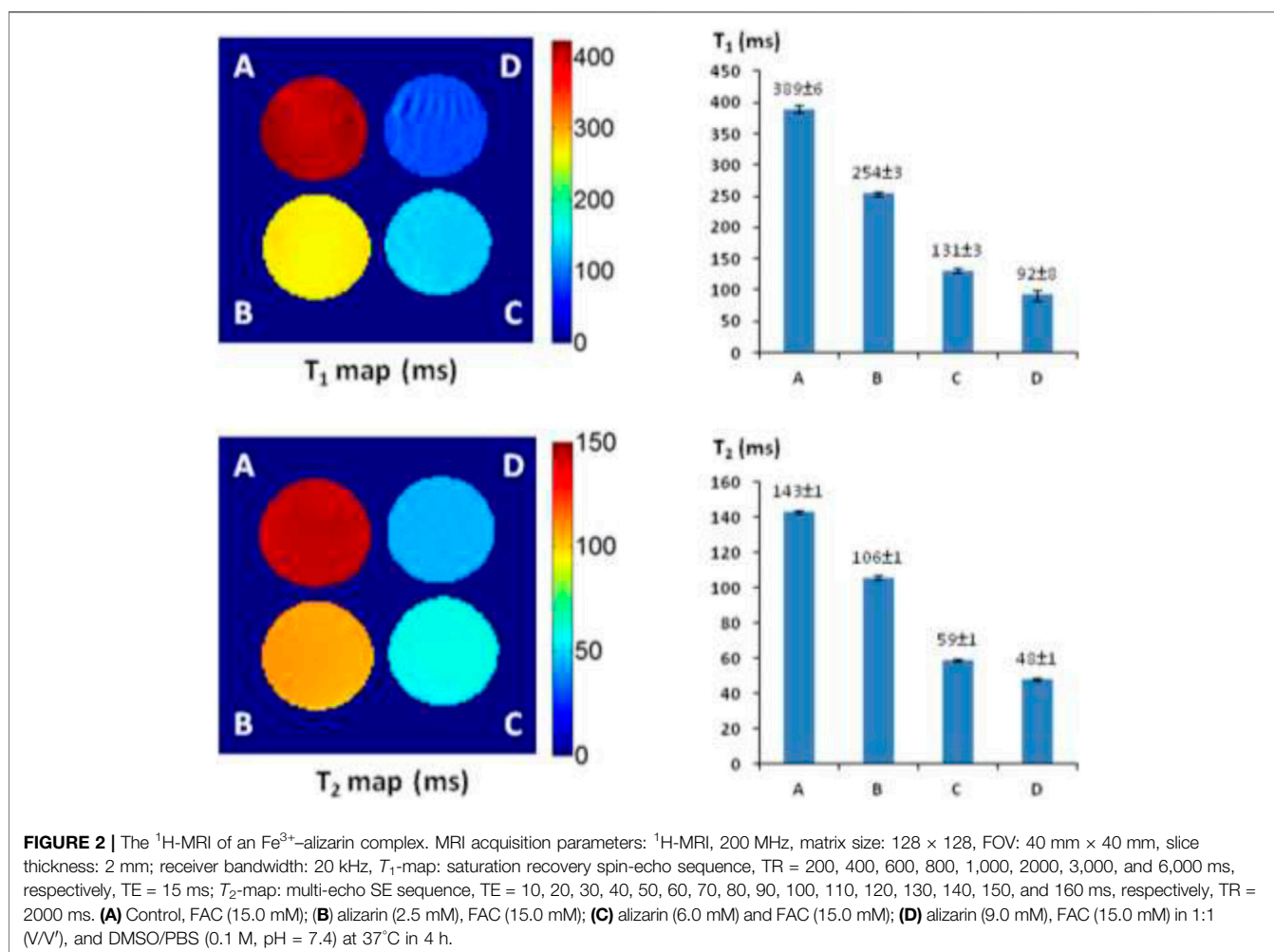
Due to various advantages such as stability, high turnover rate, and ease of conjugation, the *lacZ* gene-encoding  $\beta$ -galactosidase ( $\beta$ -gal) has been broadly used in cellular/molecular biology, small animal studies, clinical trials with assays of clonal insertion, transcriptional activation, and protein expression and interaction (Kruger et al., 1999; Haberkorn et al., 2005; Razgulin et al., 2011; Yang et al., 2019). Moreover, overexpressed  $\beta$ -gal has been identified as a vital enzyme biomarker related to cell senescence and cancer progression (Chatterjee et al., 1979; Alam et al., 1990; Dimri et al., 1995; Paradis et al., 2001; Pacheco-Rivera et al., 2016; Lozano-Torres et al., 2017; Sharma and Leblanc, 2017; Kim et al., 2018; Wang et al., 2019; Li et al., 2020b; Gao et al., 2020; Qiu et al., 2020). Thus,  $\beta$ -gal activity detection has been exploited with diverse techniques including colorimetric assays (James et al., 2000; Browne et al., 2010; Zeng et al., 2012; Yeung et al., 2013; Chen et al., 2016; Hu Q. et al.,

**Abbreviations:** NMR, nuclear magnetic resonance; MRS, magnetic resonance spectroscopy; MRI, magnetic resonance imaging; TR, repetition time; TE, echo time;  $\beta$ -gal,  $\beta$ -galactosidase; FAC, ferric ammonium citrate, TBAB, tetrabutylammonium bromide;  $\text{CH}_2\text{Cl}_2$ , dichloromethane; HRMS, high-resolution mass spectrometry; PBS, phosphate-buffered saline; X-Gal, 5-bromo-4-chloro-3-indolyl- $\beta$ -D-galactopyranoside; S-Gal, 3,4-cyclohexenoesuleitin  $\beta$ -D-galactopyranoside; DMSO, dimethyl sulfoxide; TLC, thin-layer chromatography.



2017), fluorescence (Tung et al., 2004; Urano et al., 2005; Josserand et al., 2007; Kamiya et al., 2007; Feng et al., 2009; Koide et al., 2009; Kamiya et al., 2011; Oushiki et al., 2012; Han et al., 2013; Sakabe et al., 2013; Lee et al., 2014; Asanuma et al., 2015; Peng et al., 2015; Zeng et al., 2015; Doura et al., 2016; Gu et al., 2016; Zhang C. et al., 2016; Zhang X. X. et al., 2016; Huang J. et al., 2017; Hu Q. et al., 2017; Jiang et al., 2017; Kim et al., 2017; Nakamura et al., 2017; Wei et al., 2017; Zhang et al., 2017; Tang et al., 2017; Chen et al., 2018; Ito et al., 2018; Liu et al., 2018; Yang et al., 2018; Chen et al., 2019; Fu et al., 2019; Gu et al., 2019; Jiang et al., 2019; Kong et al., 2019; Lee et al., 2019; Shi et al., 2019; Singh et al., 2019; Zhang et al., 2019a; Zhang X. et al., 2019; Zhao et al., 2019; Li et al., 2020a; Li Y. et al., 2020; Li Z. et al., 2020; Pang et al., 2020; Wu et al., 2020; Zhu et al., 2020), chemiluminescence (Wehrman et al., 2006; Liu and Mason, 2010; Broome et al., 2015; Green et al., 2017; Huang Y. et al., 2017; Wang et al., 2017; Gorai and Maitra, 2018; Hananya and Shabat, 2019; Lozano-Torres et al., 2019; Zhang et al., 2019b), positron emission tomography or single-photon emission computed tomography (Celen et al., 2008; Van Dort et al., 2008; Rempel et al., 2017), magnetic resonance imaging (MRI) (Louie et al., 2000; Chang et al., 2007; Hanaoka et al., 2008; Cui et al., 2010; Bengtsson et al., 2010; Arena et al., 2011; Yu et al., 2012a; Gulaka et al., 2013; Li et al., 2013; Heffern et al., 2014; Burke et al., 2015; Hingorani et al., 2015; Fernández-Cuervo et al., 2016; Hu J. et al., 2017; Li and Meade, 2019; Xu et al., 2019; Lilley et al., 2020), and  $^{19}\text{F}$ -MRS/MRI approaches (Yu et al., 2005; Kodibagkar et al., 2006; Yu et al., 2006; Yu and Mason, 2006; Liu et al., 2007; Yu et al., 2008a; Yu et al., 2008b; Mizukami et al., 2011; Yu et al., 2012b; Yu et al., 2013; Yu et al., 2017). In particular,  $^1\text{H}$ -MRI molecular imaging approaches for visualization of  $\beta$ -gal activity attract much more attention because  $^1\text{H}$ -MRI is noninvasive and capable of soft tissue delineation with a high lateral and depth resolution (Terreno et al., 2010; Haris et al., 2015; Wahsner et al., 2019).

$\beta$ -Galactosidase prompts the hydrolysis of  $\beta$ -D-galactopyranoside by cleavage of its  $\beta$ -anomeric C-O linkage between  $\beta$ -D-galactopyranose and aglycone; the hydrolysis reactivity of  $\beta$ -D-galactopyranosides to  $\beta$ -gal is completely dependent upon the aglycone structure. However, the structure activity relationship of the aglycones in  $\beta$ -D-galactopyranosides vs.  $\beta$ -gal is not yet clear (Juers et al., 2012; Duo et al., 2017). Therefore, further exploration is still highly needed to discover effective  $\beta$ -gal substrates for functional molecular imaging probes. We believe that the traditional histopathological methods of assaying  $\beta$ -gal activity might be the fruitful resources for developing novel imaging agents for the assessment of *lacZ* gene expression. In reviewing the histopathological literature, we noticed that the well-established  $\beta$ -gal substrate alizarin 2-O- $\beta$ -D-galactopyranoside **AZ-1** (Figure 1) is readily hydrolyzed by  $\beta$ -gal to release aglycone alizarin, which chelates with ferric iron  $\text{Fe}^{3+}$  to form an intense dark violet Fe complex (James et al., 2000). By comparison of the structural characteristics of the  $\text{Fe}^{3+}$ -alizarin complex with  $\text{Fe}^{3+}$ -based  $^1\text{H}$ -MRI contrast agents (Davies et al., 1996; Richardson et al., 1999; Schwert et al., 2002; Schwert et al., 2005; Haas and Franz, 2009; Yu et al., 2012a; Yu et al., 2012b; Gulaka et al., 2013; Li et al., 2013; Yu et al., 2013; Kuznik and Wyskocka, 2016), we speculated that the  $\text{Fe}^{3+}$ -alizarin complex could function as an  $\text{Fe}^{3+}$ -based  $^1\text{H}$ -MRI contrast agent. If so, the well-established  $\beta$ -gal substrate **AZ-1** could work as a *lacZ* gene or  $\beta$ -gal  $^1\text{H}$ -MRI reporter. Upon delivery and cleavage at *lacZ*-transfected or  $\beta$ -gal-overexpressed tumor cells with the presence of  $\text{Fe}^{3+}$ , the paramagnetic Fe complex could be spontaneously formed *in situ* and specifically produced the  $^1\text{H}$  MRI contrast effect while localizing and accumulating  $^1\text{H}$ -MRI signals at the  $\beta$ -gal activity site. Figure 1 depicts the  $\text{Fe}^{3+}$ -alizarin complex generated *in situ* for the  $^1\text{H}$ -MRI detection of  $\beta$ -gal activity. We now demonstrate the use of exploiting **AZ-1** to assess  $\beta$ -gal activity *in vitro* with *lacZ*-transfected human MCF7 breast and PC3 prostate cancer cells by  $^1\text{H}$  MRI  $T_1$  and  $T_2$  relaxation mapping.



## RESULTS AND DISCUSSION

### Verification of the $\text{Fe}^{3+}$ -Alizarin Complex as an $^1\text{H}$ -MRI Contrast Agent

Alizarin is 1,2-dihydroxy-9,10-antraquinone with a tricyclic aromatic planar structure and chelates with  $\text{Fe}^{3+}$  to form a thermodynamically stable octahedral  $\text{Fe}^{3+}$ -alizarin (1:3) complex at physiological pH conditions with the stability constant  $\log\beta = 32.21$  (Das et al., 1995; Das et al., 2002). To explore the MRI signal-enhancing capability of the  $\text{Fe}^{3+}$ -alizarin complex, the spin-lattice relaxation time  $T_1$  and spin-spin relaxation time  $T_2$  of the  $\text{Fe}^{3+}$ -alizarin complex were measured with a 4.7 T MR scanner using a saturation recovery spin echo sequence and multi-spin echo sequence with varying repetition times (TRs) and echo times (TEs), respectively. The images were acquired using a 3-cm diameter solenoid coil (home-built) with  $4 \times 4$  cut section of a 96-well plate containing the different concentrations of alizarin and ferric ammonium citrate (FAC) mixed solutions in 1:1 (V/V') DMSO/PBS (0.1 M, pH = 7.4) at 37°C. **Figure 2** displays the significant changes as expected on the  $T_1$  and  $T_2$  maps and relaxation time values of the  $\text{Fe}^{3+}$ -alizarin complex at  $T_1 = 254 \pm 3$ ,  $131 \pm 3$ , and  $92 \pm 8$  ms, and  $T_2 = 106 \pm 1$ ,

$59 \pm 1$ , and  $48 \pm 1$  ms, corresponding to the concentrations of alizarin at 2.5, 6.0, and 9.0 mM, respectively. The comparison with the control FAC of  $T_1 = 389 \pm 6$  ms and  $T_2 = 143 \pm 1$  ms showed that the  $\text{Fe}^{3+}$ -alizarin complex formed *in situ* resulted in substantial signal enhancement on either  $T_1$ - or  $T_2$ -weighted  $^1\text{H}$ -MRI, confirming the  $\text{Fe}^{3+}$ -alizarin complex generated *in situ* to function as an  $^1\text{H}$ -MRI contrast agent. Notably, the significantly different  $T_1$  and  $T_2$  values of the  $\text{Fe}^{3+}$ -alizarin complex suggested the potential to combine  $T_1$  and  $T_2$  data for additional information of imaging evaluation and detection reliability, specifically where there is possibility for misinterpretation in tissue heterogeneity (Zhou et al., 2017).

### Alizarin $\beta$ -D-Galactopyranoside Synthesis

After the  $\text{Fe}^{3+}$ -alizarin complex was shown to be an  $^1\text{H}$ -MRI contrast agent, we therefore began the  $\beta$ -D-galactopyranosylation with alizarin at the phenolic hydroxyl groups. Previously, James et al. (2000) reported a modified method for the synthesis of **AZ-1**, involving the reaction of alizarin potassium salt with acetobromo- $\alpha$ -D-galactose *via* the nucleophilic substitution procedure followed by deacetylation mediated by the aqueous NaOH solution, but the yield was low (14%). We observed that

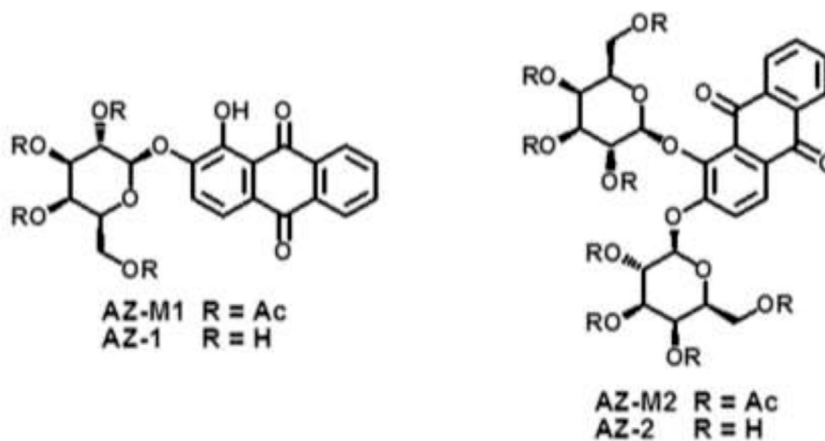


**FIGURE 3** | The structures of alizarin mono  $\beta$ -D-galactopyranosides **AZ-M1/AZ-1**, and alizarin di- $\beta$ -D-galactopyranosides **AZ-M2/AZ-2**.

the phenolic hydroxyl groups at 1,2-positions of alizarin have excellent site-reaction selectivity due to the various electronic deficiency/sterically hindered effects (Mahal et al., 2011) and apparently different  $pK_a$  values:  $pK_{a(2-OH)} = 5.98 \pm 0.05$ , whereas  $pK_{a(1-OH)} = 9.88 \pm 0.05$  (Das et al., 1995; Das et al., 2002), which suggested that the phase-transfer catalysis method at pH = 8–9 could provide regio- and stereoselective synthesis of **AZ-1**, as exploited previously for  $\beta$ -gal  $^{19}\text{F}$ -MRS/MRI reporters (Yu et al., 2005; Kodibagkar et al., 2006; Yu et al., 2006; Yu and Mason, 2006; Liu et al., 2007; Yu et al., 2008a; Yu et al., 2008b; Yu et al., 2012b; Yu et al., 2013; Yu et al., 2017). To the well-stirred solution of alizarin in  $\text{CH}_2\text{Cl}_2$ - $\text{H}_2\text{O}$  (pH 8–9) using tetrabutylammonium bromide (TBAB) as a catalyst at 50°C, an equimolar amount of 2, 3, 4, and 6-tetra-*O*-acetyl- $\alpha$ -D-galactopyranosyl bromide was dropped under  $\text{N}_2$  atmosphere for around 1 h; alizarin 2-*O*-2', 3', 4', and 6'-tetra-*O*-acetyl- $\beta$ -D-galactopyranoside **AZ-M1** was isolated purely at the yield of 78%. The NOESY correlation between anomeric H-1' and H-3 in **AZ-M1** (Supporting Information, **Supplementary Figure S7**) showed that  $\beta$ -D-galactopyranosylation took place at the 2-hydroxyl group of alizarin as predicted. The following deacetylation with  $\text{NH}_3/\text{MeOH}$  from 0°C to room temperature produced **AZ-1** at 91% yield.

The prerequisite for molecular MRI of intracellular targets is that the contrast agents must be effectively taken up by cells *in vivo*, which requires contrast agents to be sufficiently soluble and capable of entering cells. Carbohydrate-associated prodrugs in clinical applications have widely demonstrated the improved aqueous solubility and permeability, leading to better selectivity and efficacy for diagnosis and therapy (Dwek, 1996; Bertozzi and Kiessling, 2001; Hudak and Bertozzi, 2014; Fernández-Tejada et al., 2015). We hence thought about introducing an additional  $\beta$ -D-galactopyranosyl unit to form alizarin 1,2-di-*O*- $\beta$ -D-galactopyranoside **AZ-2**. Similarly, a drop of 2.2 equivalent 2, 3, 4, and 6-tetra-*O*-acetyl- $\alpha$ -D-galactopyranosyl bromide  $\text{CH}_2\text{Cl}_2$  solution into alizarin in  $\text{CH}_2\text{Cl}_2$ - $\text{H}_2\text{O}$  (pH 10–11) employing TBAB as a catalyst at 55°C under  $\text{N}_2$  atmosphere afforded

alizarin 1,2-di-*O*-2', 3', 4', 6'-tetra-*O*-acetyl- $\beta$ -D-galactopyranoside **AZ-M2** at 62% yield. Deacetylation accomplished the target molecule alizarin 1,2-di-*O*- $\beta$ -D-galactopyranoside **AZ-2** with 94% yield. **Figure 3** illustrates the structures of **AZ-1/AZ-M1** and **AZ-2/AZ-M2**. As expected, the free di- $\beta$ -D-galactopyranoside **AZ-2** is soluble in PBS (0.1 M, pH = 7.4) at the concentration of 15 mM; meanwhile, the free mono- $\beta$ -D-galactopyranoside **AZ-1** unlikely requires the addition of DMSO for the same concentration. The structures of **AZ-M1/AZ-1** and **AZ-M2/AZ-2** were confirmed by NMR and HRMS data. The molecular/quasimolecular ions of **AZ-M1** and **AZ-1**, as well as **AZ-M2** and **AZ-2**, showed the introduction of one and two galactopyranosyl units to **AZ-M1/AZ-1** and **AZ-M2/AZ-2**, respectively, in which the  $\beta$ -D-galactopyranoside configuration was determined by  $1\text{H}/^{13}\text{C}$  NMR data of the anomeric protons at  $\delta_{\text{H-1}'} = \delta_{\text{H-1}''} = 4.90$ –5.30 ppm and their coupling constants  $J_{1',2'} = J_{1'',2''} \approx 8.0$  Hz while maintaining the corresponding anomeric C-1'/C-1'' at  $\delta_{\text{C-1}'} = \delta_{\text{C-1}''} = 99.5$ –104.0 ppm in accordance (Supporting Information, **Supplementary Figures S4–S13**), which are in agreement with the typical characteristics for the identification of the anomeric  $\beta$ -D-configuration (Yu et al., 2005; Yu et al., 2006; Yu and Mason, 2006; Kodibagkar et al., 2006; Liu et al., 2007; Yu et al., 2008a; Yu et al., 2008b; Yu et al., 2012b; Yu et al., 2013; Yu et al., 2017).

### $\beta$ -Gal Reactivity

**AZ-1** has been identified as a highly sensitive substrate for the demonstration of  $\beta$ -gal in a range of Gram-negative bacteria under incubation at 37°C in air for 18 h (James et al., 2000). However, none of the existing data have shown the kinetics of **AZ-1** vs.  $\beta$ -gal, which is crucial for further *in vivo* imaging applications. The absorption spectra of **AZ-1** and **AZ-2** solutions in 1:1 (V/V') DMSO/PBS (0.1 M, pH = 7.4) with and without  $\beta$ -gal (E801A) at 20–22°C indicated that upon reactions of **AZ-1** and **AZ-2** with  $\beta$ -gal, a new absorption around 520 nm, corresponding to the *in situ* released alizarin mono-/dianions, appeared and increased gradually. Hence, the absorbance measurements at 520 nm following the enzymatic

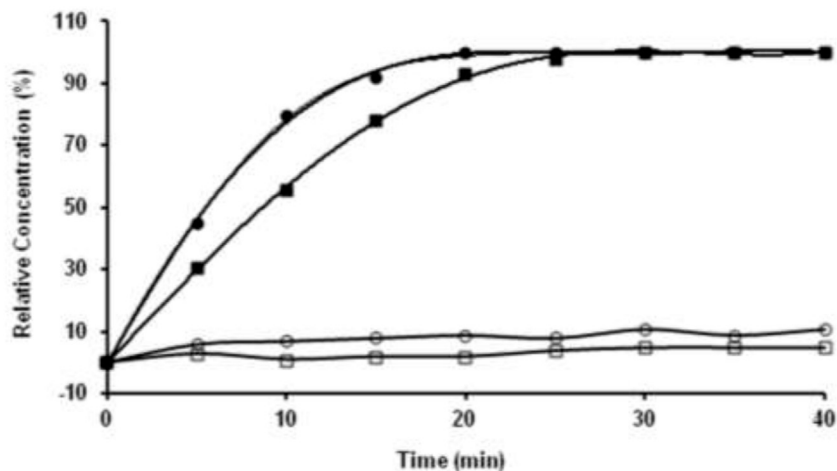


**FIGURE 4 |** The kinetic hydrolysis time courses of alizarin  $\beta$ -D-galactopyranosides **AZ-1** (■) and **AZ-2** (●) with  $\beta$ -gal. Absorbance measurements at  $\lambda = 520$  nm following the addition of  $\beta$ -gal (E801A, 3 units) to solutions of **AZ-1**, **AZ-2** each (5.0 mM) in 1:1 (V/V) DMSO/PBS (0.1 M, pH = 7.4) at 20–22°C in different time points; The time courses of alizarin  $\beta$ -D-galactopyranosides **AZ-1** (□) and **AZ-2** (○) each (5.0 mM) in 1:1 (V/V) DMSO/PBS (0.1 M, pH = 7.4) at 20–22°C in different time points without  $\beta$ -gal (E801A).

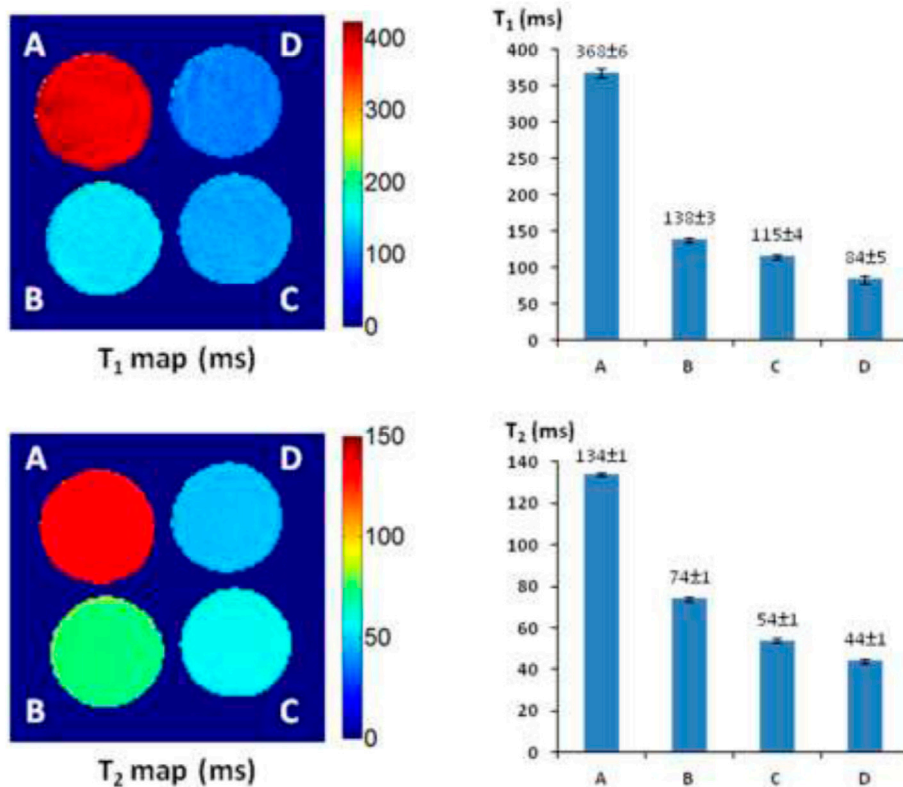


**FIGURE 5 |**  $^1\text{H}$ -MRI detection of  $\beta$ -gal activity.  $^1\text{H}$ -MRI acquisition: using the same parameters as in **Figure 2**, **(A)** alizarin 2-O- $\beta$ -D-galactopyranoside **AZ-1** (9.0 mM) and FAC (15.0 mM); **(B)** alizarin 2-O- $\beta$ -D-galactopyranoside **AZ-1** (4.0 mM), FAC (15.0 mM), and  $\beta$ -gal (E801A, 5 units); **(C)** alizarin 2-O- $\beta$ -D-galactopyranoside **AZ-1** (6.0 mM), FAC (15.0 mM), and  $\beta$ -gal (E801A, 5 units); **(D)** alizarin 2-O- $\beta$ -D-galactopyranoside **AZ-1** (9.0 mM), FAC (15.0 mM), and  $\beta$ -gal (E801A, 5 units) in 1:1 (V/V) DMSO/PBS (0.1 M, pH = 7.4) at 37°C in 4 h.

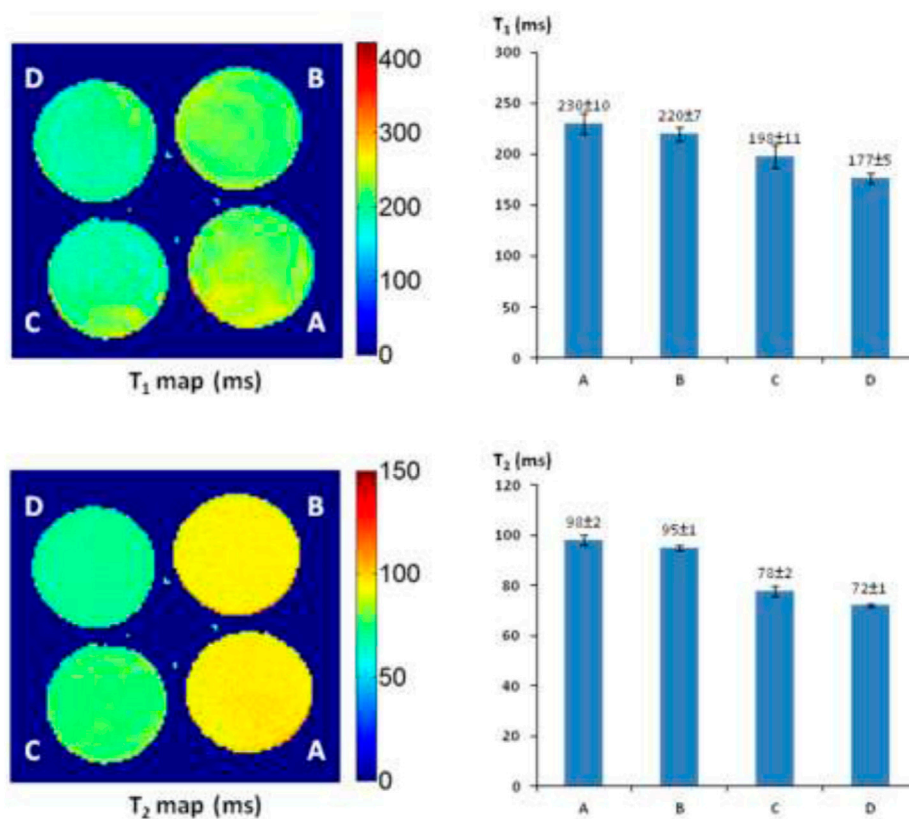


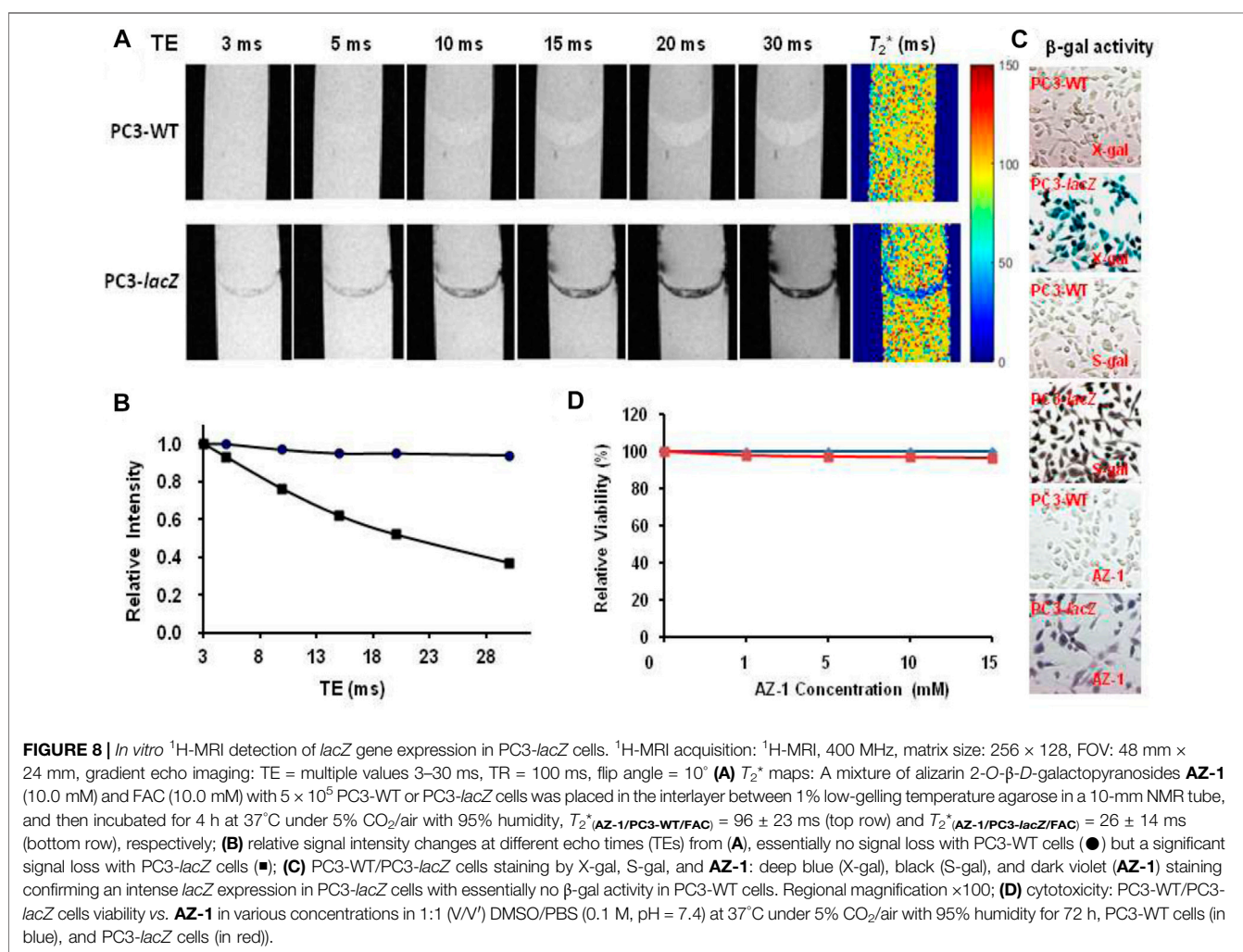
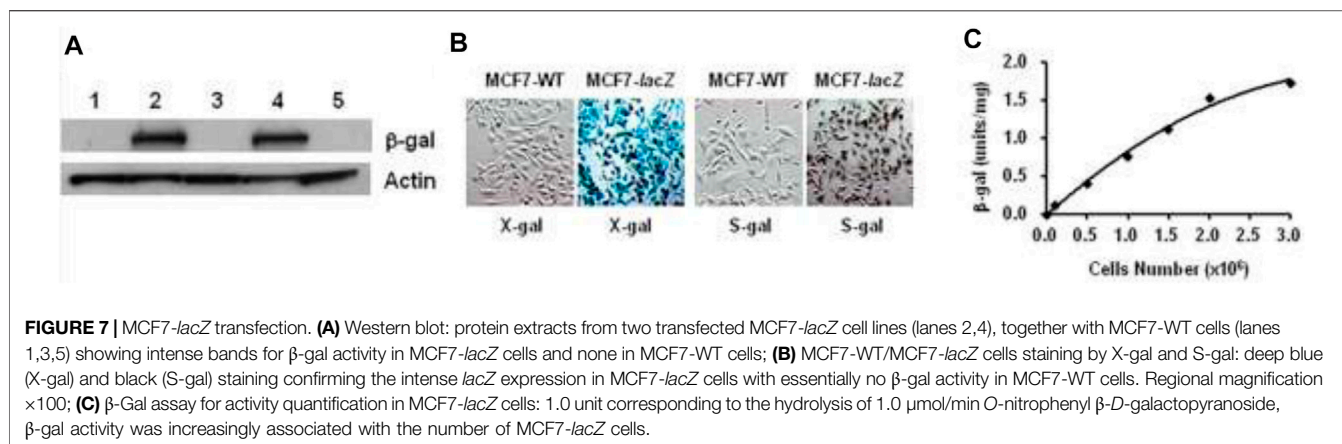
**FIGURE 6** |  $^1\text{H}$ -MRI detection of  $\beta$ -gal activity.  $^1\text{H}$ -MRI acquisition: using the same parameters as in **Figure 2**, (A) alizarin 1,2-di-*O*- $\beta$ -*D*-galactopyranoside **AZ-2** (9.0 mM) and FAC (15.0 mM); (B) alizarin 1,2-di-*O*- $\beta$ -*D*-galactopyranoside **AZ-2** (4.0 mM), FAC (15.0 mM), and  $\beta$ -gal (E801A, 5 units); (C) alizarin 1,2-di-*O*- $\beta$ -*D*-galactopyranoside **AZ-2** (6.0 mM), FAC (15.0 mM), and  $\beta$ -gal (E801A, 5 units); (D) alizarin 1,2-di-*O*- $\beta$ -*D*-galactopyranoside **AZ-2** (9.0 mM), FAC (15.0 mM), and  $\beta$ -gal (E801A, 5 units) in 1:1 (V/V') DMSO/PBS (0.1 M, pH = 7.4) at 37°C in 4 h.

reaction of **AZ-1** and **AZ-2** with  $\beta$ -gal (E801A) at 20–22°C in different time points showed that both **AZ-1** and **AZ-2** are very reactive to  $\beta$ -gal (E801A) with varying hydrolytic rates at  $v_{(\text{AZ-1})} = 93.3$  and  $v_{(\text{AZ-2})} = 133.3 \mu\text{M}/\text{min}/\text{unit}$ , respectively (**Figure 4**). Also, the absorption spectra of **AZ-1** and **AZ-2** by reaction with other enzymes  $\alpha$ -galactosidase (Sigma G7163) and  $\beta$ -glucuronidase (Sigma G8295) at 20–22°C; showed that both **AZ-1** and **AZ-2** remained essentially stable over the period of 60 min, verifying their specificity for reaction to  $\beta$ -gal.

### $^1\text{H}$ -MRI Detection of $\beta$ -Gal Activity

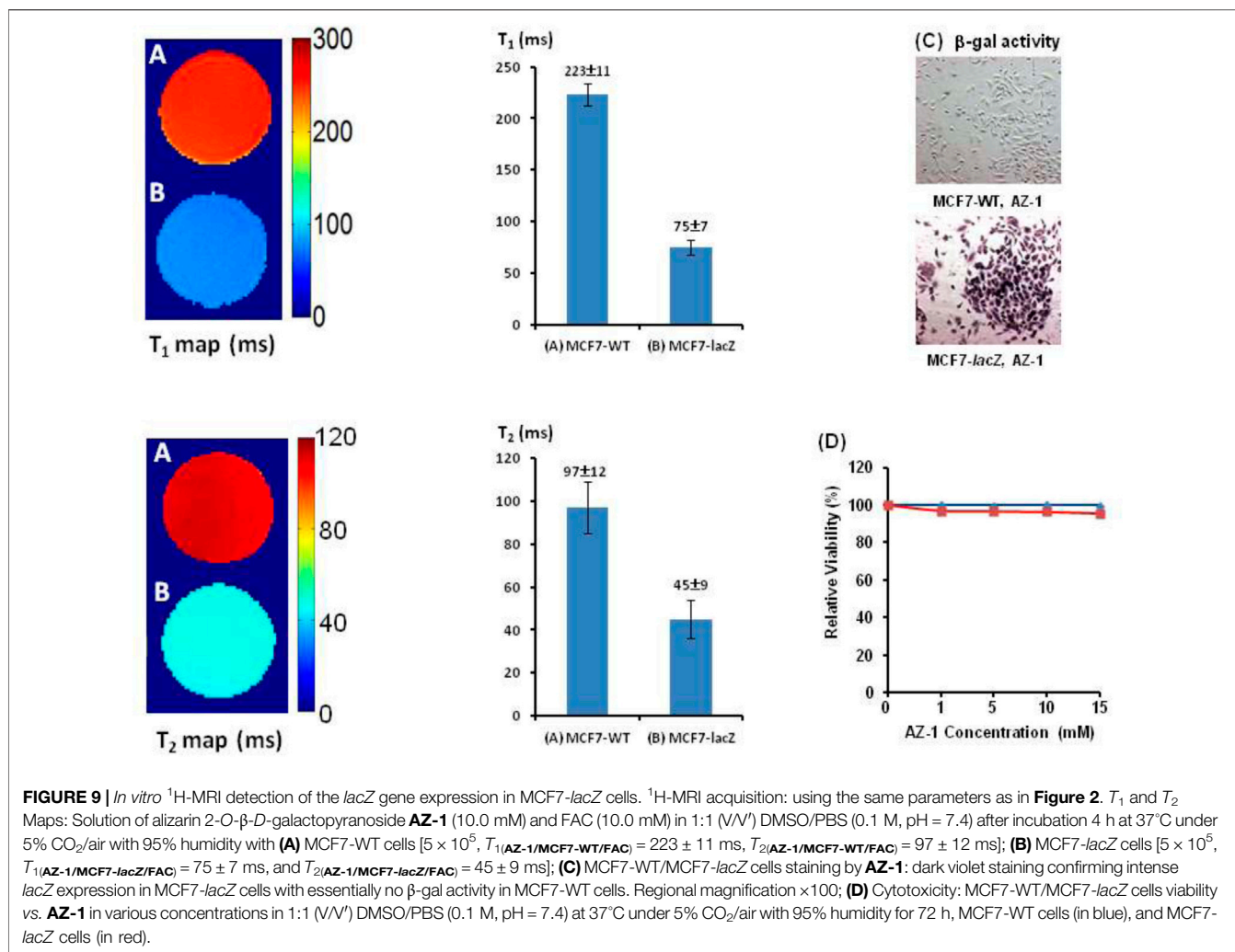
The  $T_1$  and  $T_2$  maps and relaxation time values were measured with a  $4 \times 4$  cut section of 96-well plate containing various concentrations of **AZ-1** and **AZ-2** (4.0–9.0 mM) together with a fixed concentration of FAC (15.0 mM), respectively, in 1:1 (V/V') DMSO/PBS (0.1 M, pH = 7.4) with or without  $\beta$ -gal (E801A). In the **AZ-1**/FAC solution at 37°C in 4 h in the absence of  $\beta$ -gal, relaxation times were determined to be  $T_1 = 368 \pm 6$  and  $T_2 = 134 \pm 1$  ms. In comparison, in the presence of  $\beta$ -gal (E801A, 5 units) in the mixture solution of **AZ-1** and FAC at 37°C in 4 h, pronounced shortening in relaxation times  $T_1$  and  $T_2$  caused by the  $\text{Fe}^{3+}$ -alizarin complex generated *in situ* was observed at  $T_1 = 138 \pm 3$ ,  $115 \pm 4$ , and  $84 \pm 5$  ms, whereas  $T_2 = 74 \pm 1$ ,  $54 \pm 1$ , and

$44 \pm 5$  ms, correlating with the increasing concentrations of **AZ-1** from 4.0, 6.0 and 9.0 mM, respectively (**Figure 5**). However, the much more soluble and reactive **AZ-2**, exhibiting significant advantages for *in vivo*  $^1\text{H}$ -MRI applications, produced very unexpected results under similar procedures at the same conditions. In the absence of  $\beta$ -gal at 37°C in 4 h, the **AZ-2**/FAC solution, as the control, yielded surprisingly reduced  $T_1 = 230 \pm 11$  and  $T_2 = 98 \pm 1$  ms (**Figure 6**). However, in the presence of  $\beta$ -gal (E801A, 5 units), the mixture solutions of **AZ-2**/FAC gave rise to an insignificant decrease in  $T_1 = 220 \pm 7$ ,  $198 \pm 11$ , and  $177 \pm 5$  ms and  $T_2 = 95 \pm 1$ ,  $78 \pm 2$ , and  $72 \pm 1$  ms (**AZ-2** concentrations at 4.0, 6.0, and 9.0 mM, respectively, **Figure 6**), indicating the much less  $\text{Fe}^{3+}$ -alizarin complex formed *in situ* during the  $\beta$ -gal hydrolysis. Comparing the interactions between **AZ-1**/**AZ-2** and  $\text{Fe}^{3+}$  with their relaxivities to FAC, we attributed that the larger differences of **AZ-2**/FAC to FAC solution ( $T_1$ :  $230 \pm 11$  vs.  $389 \pm 6$  ms and  $T_2$ :  $98 \pm 1$  vs.  $143 \pm 1$  ms; alternatively,  $\Delta R_1 = 1.78 \text{ s}^{-1}$  and  $\Delta R_2 = 3.21 \text{ s}^{-1}$ ) than **AZ-1**/FAC solution ( $T_1$ :  $368 \pm 6$  vs.  $389 \pm 6$  ms,  $T_2$ :  $134 \pm 1$  vs.  $143 \pm 1$  ms; alternatively,  $\Delta R_1 = 0.15 \text{ s}^{-1}$ ,  $\Delta R_2 = 0.47 \text{ s}^{-1}$ ) were risen from the formation of the much stronger and more stable molecular tweezer complex **AZ-2**/ $\text{Fe}^{3+}$  due to the adjacent 3',4',6'-OH and 3'',4'',6''-OH located at the same side of 1,2-



di-*O*- $\beta$ -*D*-galactopyranosyl rings in the favored configuration for chelation of  $\text{Fe}^{3+}$  (**Supplementary Figure S3** in the Supporting Information) (Davies et al., 1996; Richardson et al., 1999; Schwert et al., 2002; Schwert et al., 2005; Haas and Franz, 2009; Coskuner et al., 2011; Kuznik and Wyskocka, 2016) which thus

simultaneously hindered the reaction with  $\beta$ -gal (E801A) and slowed down the release of alizarin as well as the *in situ* generation of the  $\text{Fe}^{3+}$ -alizarin complex. These were confirmed by mixing solutions of **AZ-2** and  $\beta$ -gal (E801A) first for hydrolysis, and then followed by adding FAC for



complexation at 37°C in 2 h for each step with the same concentrations as in **Figure 6**. A significant decrease in relaxation times  $T_1$  and  $T_2$  was seen at  $T_1 = 133 \pm 1$ ,  $110 \pm 2$ , and  $78 \pm 2$  ms and  $T_2 = 73 \pm 2$ ,  $51 \pm 3$ , and  $41 \pm 1$  ms, which were very close to expectations based on **AZ-1/FAC**  $T_1$  and  $T_2$  data as shown in **Figure 5**.

### **In Vitro** $^1\text{H}$ -MRI Detection of *lacZ* Transfection in Human Tumor Cells

The recombinant vector  $\text{pCMVlacZ}$  has been successfully created and used to stably transfect human prostate cancer PC3-*lacZ* cells from PC3-wild-type (WT) cells (Liu et al., 2007). Accordingly, human breast cancer MCF7-*lacZ* cells were stably transfected from MCF7 wild-type (WT) cells: the  $\beta$ -gal activity and quantification in MCF7-*lacZ* cells were verified on the basis of Western blot, X-gal and S-gal staining, and the  $\beta$ -gal assay (**Figure 7**).

Given **AZ-2** showed much better aqueous solubility and reactivity to  $\beta$ -gal, the stabilized molecular tweezer complexation **AZ-2/Fe $^{3+}$**  obstructed its implementation spreading to effective  $^1\text{H}$ -MRI assessment of  $\beta$ -gal. So, **AZ-1** with a significant signal

loss either on  $T_1$  or  $T_2$  upon  $\beta$ -gal hydrolysis was prompted for the further *in vitro*  $^1\text{H}$ -MRI evaluation. As an initial demonstration for *in vitro*  $^1\text{H}$ -MRI detection of  $\beta$ -gal with *lacZ*-transfected human cancer cells, we first acquired  $T_2^*$  maps on pair mixtures of **AZ-1** (10.0 mM) with PC3-WT cells ( $5 \times 10^5$ ) and PC3-*lacZ* cells ( $5 \times 10^5$ ), respectively, in the presence of FAC (10.0 mM) layered between agarose after incubation 4 h at 37°C under 5%  $\text{CO}_2$ /air with 95% humidity. Significant differences confined within the layers were observed between PC3-WT and PC3-*lacZ* cells at different echo times (**Figure 8A**), in which there was essentially no signal loss with PC3-WT cells but a remarkable signal decrease with PC3-*lacZ* cells upon increasing echo times (TEs) (**Figure 8B**). The relaxation time  $T_2^*$  was determined to be  $T_2^*(\text{AZ-1/PC3/FAC}) = 96 \pm 23$  ms in PC3-WT cells, while  $T_2^*(\text{AZ-1/PC3-*lacZ*/FAC}) = 26 \pm 14$  ms in PC3-*lacZ* cells. Again, the  $\beta$ -gal activity was verified based on X-gal, S-gal, and **AZ-1** staining (dark violet) (**Figure 8C**), with each staining method consistently showing intense *lacZ* expression in PC3-*lacZ* cells with essentially no  $\beta$ -gal activity in PC3-WT cells.

The cytotoxicity of **AZ-1** was studied with PC3-WT and PC3-*lacZ* cells in PBS (0.1 M, pH = 7.4) incubated 72 h at 37°C under

5% CO<sub>2</sub>/air with 95% humidity. Cell viability assays showed that neither **AZ-1** nor alizarin showed toxicity to PC3 cells, for **AZ-1** viability exceeded 96% for both PC3-WT and PC3-*lacZ* cells at all concentrations tested (Figure 8D).

Furthermore, *in vitro* <sup>1</sup>H-MRI acquisition of **AZ-1** (10.0 mM) with PC3-WT cells (5 × 10<sup>5</sup>) and PC3-*lacZ* cells (5 × 10<sup>5</sup>) in the presence of FAC (10.0 mM) was performed in a 1:1 (V/V') DMSO/PBS (0.1 M, pH = 7.4) solution. A pronounced signal decrease in the relaxation time *T*<sub>1</sub> was observed between PC3-WT (*T*<sub>1(AZ-1/PC3-WT/FAC)</sub> = 245 ± 9 ms) and PC3-*lacZ* cells (*T*<sub>1(AZ-1/PC3-lacZ/FAC)</sub> = 82 ± 7 ms) after incubation 4 h at 37°C under 5% CO<sub>2</sub>/air with 95% humidity.

Similarly, after incubation of **AZ-1** (10.0 mM) with MC7-WT cells (5 × 10<sup>5</sup>) and MC7-*lacZ* cells (5 × 10<sup>5</sup>), respectively, in the same conditions as the previous study, the relaxation times were observed to be *T*<sub>1(AZ-1/MCF7-WT/FAC)</sub> = 223 ± 11 ms and *T*<sub>2(AZ-1/MCF7-WT/FAC)</sub> = 97 ± 12 ms in MC7-WT cells, whereas *T*<sub>1(AZ-1/MCF7-lacZ/FAC)</sub> = 75 ± 7 ms and *T*<sub>2(AZ-1/MCF7-lacZ/FAC)</sub> = 45 ± 9 ms for MC7-*lacZ* cells (Figures 9A,B), the *T*<sub>1</sub> and *T*<sub>2</sub> values are shown as bars adjacent to *T*<sub>1</sub> and *T*<sub>2</sub> maps; both illustrated significant differences after the reaction with  $\beta$ -gal at  $\Delta R_1 = 8.85 \text{ s}^{-1}$  and  $\Delta R_2 = 11.91 \text{ s}^{-1}$ . Staining by X-gal, S-gal, and **AZ-1** (dark violet) (Figure 9C) all displayed an intense *lacZ* expression in MC7-*lacZ* cells but with essentially no  $\beta$ -gal activity in MC7-WT cells. Cell viability assays indicated that both **AZ-1** and the released aglycone alizarin have no toxicity to MC7 cells upon the viability above 95% to MC7-WT and MC7-*lacZ* cells at all concentrations tested for 72 h (Figure 9D).

Currently, a Gd-based contrast agent-enhanced <sup>1</sup>H-MRI has been widely applied for medical diagnosis, offering a noninvasive way to generate anatomical and physiological information while maintaining high spatial and temporal resolution (Terreno et al., 2010; Haris et al., 2015; Wahsner et al., 2019). An Fe-based <sup>1</sup>H MRI contrast agent, different from the Gd<sup>3+</sup>-based <sup>1</sup>H MRI contrast agent with very strong relaxivity, exhibited much shorter relaxation times because of the formation of Fe complexes with the complete coordination of Fe<sup>3+</sup>, eliminating the possibility of inner-sphere to directly coordinate water, leaving outer-sphere and second-sphere coordination water molecules as the only pathways for relaxation (Davies et al., 1996; Richardson et al., 1999; Schwert et al., 2002; Schwert et al., 2005; Haas and Franz, 2009; Kuznik and Wyskocka, 2016). However, an Fe-based contrast agent enhanced <sup>1</sup>H-MRI has now become a viable alternative because Fe<sup>3+</sup> is extensively present in the tissues of the human body and is involved in transport, storage, compartmentalization, and excretion mechanisms, while Gd<sup>3+</sup> is not naturally present in human biochemistry (Beutler, 2004; Weber et al., 2006; Kaplan and Kaplan, 2009; Theil and Goss, 2009). Particularly, cancer cells need a significant amount of Fe<sup>3+</sup> for rapid replication, so endogenously abundant Fe<sup>3+</sup> in tumors has been recognized as a molecular target for chemotherapeutic treatments through depleting cancer cellular Fe<sup>3+</sup> to disrupt cancer cell proliferation and inhibit tumor growth (Fe<sup>3+</sup>-chelation therapy) (Buss et al., 2003; Richardson, 2005). In this study, we introduced exogenous Fe<sup>3+</sup> with the ultimate goal of developing this approach to hunt the elevated Fe<sup>3+</sup> level in tumors for the <sup>1</sup>H-MRI signal generation. Indeed, alizarin has

a very high thermodynamic stability constant  $\log\beta = 32.21$  (Das et al., 1995; Das et al., 2002), indicating its capability of capturing Fe<sup>3+</sup> from tumor to produce the Fe<sup>3+</sup>-alizarin complex *in situ* while simultaneously generating the <sup>1</sup>H-MRI signal enhancement (Richardson et al., 1999; Davies et al., 1996; Schwert et al., 2002; Schwert et al., 2005; Haas and Franz, 2009; Kuznik and Wyskocka, 2016). Moreover, alizarin has been known to inhibit human cytomegalovirus replication, HIV-1 RT-associated RDDP, and integrase activities (Esposito et al., 2011). Furthermore, alizarin is the core part of anthraquinones, which constitute numerous antitumor drugs widely applied in the treatment of various neoplasms such as Adriamycin and daunorubicin, and their coordination with Fe<sup>3+</sup> was shown to diminish cardiotoxicity while improving the antitumor activity in chemotherapy and maintain sound radiosensitizing properties in radiotherapy (Lown, 1993; Nowak and Tarasiuk, 2012; Malik and Müller, 2016). Therefore, this novel molecular platform also indicates the potential for cancer therapy and imaging by utilizing the  $\beta$ -gal responsive turn on pathway to selectively deplete tumor Fe<sup>3+</sup>, resulting in cancer cell cycle arrest and apoptosis while generating <sup>1</sup>H-MRI contrast enhancement, thereby providing insight into the *lacZ* gene expression, development, location, and magnitude.

## CONCLUSION

In this study, we present a novel responsive molecular platform for  $\beta$ -gal activity detection using <sup>1</sup>H-MRI, in which the <sup>1</sup>H-MRI signal enhancement is specifically generated, localized, and accumulated *in situ* at the  $\beta$ -gal activity site. In conjunction with this design, we have successfully produced and characterized alizarin 2-O- $\beta$ -D-galactopyranoside **AZ-1** and alizarin 1,2-di-O- $\beta$ -D-galactopyranoside **AZ-2**. We have also demonstrated the feasibility of using **AZ-1** by spontaneous *in situ* formation of paramagnetic Fe<sup>3+</sup>-alizarin complex to assess the  $\beta$ -gal activity in solution with Fe<sup>3+</sup> ions existence by <sup>1</sup>H-MRI *T*<sub>1</sub> and *T*<sub>2</sub>/*T*<sub>2</sub>\* relaxation mapping. <sup>1</sup>H-MRI clearly showed the significant differences in both *T*<sub>1</sub> and *T*<sub>2</sub> at WT vs. *lacZ* gene expressing cells in culture after incubation with **AZ-1**, signifying the potential of integrating *T*<sub>1</sub> and *T*<sub>2</sub> data together to gain the additional certainty in imaging evaluation and detection reliability of  $\beta$ -gal activity.

## EXPERIMENTAL

### General Methods

NMR spectra were recorded on a Varian Unity INOVA 400 spectrometer (400 MHz for <sup>1</sup>H, 100 MHz for <sup>13</sup>C). <sup>1</sup>H and <sup>13</sup>C chemical shifts are referenced to TMS as an internal standard with CDCl<sub>3</sub>, or DMSO-*d*<sub>6</sub> as solvents, and chemical shifts are given in ppm. All compounds were characterized by NMR at 25°C. Mass spectra were obtained by positive and negative ESI-MS using a Micromass Q-TOF hybrid quadrupole/time-of-flight instrument (Micromass UK Ltd.). Absorption spectra were taken on a UV-2700 UV-Vis Shimadzu spectrophotometer.

Solutions in organic solvents were dried with anhydrous sodium sulfate and concentrated *in vacuo* below 45°C. 2, 3, 4, 6-Tetra-*O*-acetyl- $\alpha$ -*D*-galactopyranosyl bromide was purchased from the Sigma Chemical Company.  $\beta$ -Gal (E801A) was purchased from the Promega (Madison, WI, United States), and enzymatic reactions were performed at 37°C in the PBS solution (0.1 M, pH = 7.4). Column chromatography was performed on silica gel (200–300 mesh), and silica gel GF<sub>254</sub> used for analytical TLC was purchased from the Aldrich Chemical Company. The detection was affected by spraying the plates with 5% ethanolic H<sub>2</sub>SO<sub>4</sub> (followed by heating at 110°C for 10 min) or by direct UV illumination of the plate. The purity of the final products was determined by HPLC with  $\geq$ 95%.

### Alizarin 2-*O*-2', 3', 4', 6'-Tetra-*O*-Acetyl- $\beta$ -*D*-Galactopyranoside AZ-M1

A solution of 2, 3, 4, 6-tetra-*O*-acetyl- $\alpha$ -*D*-galactopyranosyl bromide (1.23 g, 3.0 mmol) in CH<sub>2</sub>Cl<sub>2</sub> (15 ml) was added dropwise to a vigorously stirred CH<sub>2</sub>Cl<sub>2</sub>-H<sub>2</sub>O biphasic mixture (pH 8–9) of alizarin (0.72 g, 3.0 mmol) and tetrabutylammonium bromide (TBAB) (322 mg, 1.0 mmol) in CH<sub>2</sub>Cl<sub>2</sub>-H<sub>2</sub>O (30 ml, 1:1 V/V') around 1 h at 50°C under N<sub>2</sub> atmosphere, with stirring continued for an additional 4–5 h until TLC showed that the reaction was completed. The product was extracted with CH<sub>2</sub>Cl<sub>2</sub> (4  $\times$  30 ml) and subsequently washed (H<sub>2</sub>O), dried (Na<sub>2</sub>SO<sub>4</sub>), and evaporated under reduced pressure to give a syrup, which was purified by column chromatography on silica gel to give alizarin 2-*O*-2', 3', 4', 6'-tetra-*O*-acetyl- $\beta$ -*D*-galactopyranoside **AZ-M1**.

### Alizarin 1,2-Di-*O*-2', 3', 4', 6'-Tetra-*O*-Acetyl- $\beta$ -*D*-Galactopyranoside AZ-M2

A solution of 2, 3, 4, 6-tetra-*O*-acetyl- $\alpha$ -*D*-galactopyranosyl bromide (2.71 g, 6.6 mmol) in CH<sub>2</sub>Cl<sub>2</sub> (30 ml) was added dropwise to a vigorously stirred CH<sub>2</sub>Cl<sub>2</sub>-H<sub>2</sub>O biphasic mixture (pH 10–11) of alizarin (0.72 g, 3.0 mmol) and TBAB (322 mg, 1.0 mmol) in CH<sub>2</sub>Cl<sub>2</sub>-H<sub>2</sub>O (30 ml, 1:1 V/V') around 1 h at 55°C under N<sub>2</sub> atmosphere, with stirring continued for an additional 4–5 h until TLC showed that the reaction was completed. The product was extracted with CH<sub>2</sub>Cl<sub>2</sub> (4  $\times$  40 ml) and subsequently washed (H<sub>2</sub>O), dried (Na<sub>2</sub>SO<sub>4</sub>), and evaporated under reduced pressure to give a syrup, which was purified by column chromatography on silica gel to give alizarin 1,2-di-*O*-2', 3', 4', 6'-tetra-*O*-acetyl- $\beta$ -*D*-galactopyranoside **AZ-M2**.

### Alizarin 2-*O*- $\beta$ -*D*-Galactopyranoside AZ-1 and Alizarin

#### 1,2-Di-*O*- $\beta$ -*D*-Galactopyranoside AZ-2

General procedure: A solution of alizarin 2-*O*-2', 3', 4', 6'-tetra-*O*-acetyl- $\beta$ -*D*-galactopyranoside **AZ-M1** or alizarin 1,2-di-*O*-2', 3', 4', 6'-tetra-*O*-acetyl- $\beta$ -*D*-galactopyranoside **AZ-M2** (1.30 g)

in anhydrous MeOH (120 ml) containing 0.5 M NH<sub>3</sub> was vigorously stirred from 0°C to room temperature overnight until TLC showed that the reaction was complete and then evaporated to dryness *in vacuo*. Chromatography of the crude syrup on silica gel with ethyl acetate-methanol afforded the corresponding alizarin 2-*O*- $\beta$ -*D*-galactopyranoside **AZ-1** and alizarin 1,2-di-*O*- $\beta$ -*D*-galactopyranoside **AZ-2** in high yields.

### MRI

MRI studies were performed using a 4.7T horizontal bore magnet or a 9.4T vertical bore magnet equipped with a Varian INOVA Unity system (Palo Alto, CA, United States).  $T_1$  and  $T_2$  (or  $T_2^*$ ) maps were acquired using a spin echo (or gradient echo) sequence with varying repetition times (TRs) or echo times (TEs), respectively. The raw data were acquired using a centric  $k$ -space reordering scheme, followed by the phase encoding steps with higher phase encoding gradient amplitudes. Data acquisition parameters of the FLASH readout were TR/TE/Flip angle = 10 ms/5 ms/10°. The standard multi-echo Carr–Purcell–Meiboom–Gill pulse sequence was used for measuring  $T_2$  from a single echo train. The  $T_2$  and  $T_2^*$  maps were obtained on a voxel-by-voxel basis using a nonlinear least-squares fit equation  $M = M_0 e^{-TE/T_2}$  from the images taken at each echo time. Images were reconstructed and analyzed by using MatLab (MathWorks, Natick, MA).

### *lacZ* Transfection in Human Tumor Cells

The *E. coli lacZ* gene (from pSV- $\beta$ -gal vector, Promega, Madison, WI, United States) was inserted into a high expression human cytomegalovirus (CMV) immediate early enhancer/promoter vector pHCMV (Gene Therapy Systems, San Diego, CA, United States), producing a recombinant vector pHCMV/*lacZ*. This was used to transfect wild-type MCF7 (human breast cancer) and PC3 (human prostate cancer) cells (ATCC, Manassas, VA, United States) using GenePORTER2 (Gene Therapy Systems, Genlantis, Inc., San Diego, CA, United States). The highest  $\beta$ -gal expressing colony was selected using the antibiotic G418 disulfate (800  $\mu$ g/ml, Research Products International Corp, Mt Prospect, IL, United States), and G418 (200  $\mu$ g/ml) was also included for routine culture. The cells were maintained in Dulbecco's modified Eagle's medium (DMEM, Mediatech Inc., Herndon, VA, United States) containing 10% fetal bovine serum (FBS, 0.1 M, pH = 7.4, Atlanta Biologicals, Inc., Lawrenceville, GA, United States) with 100 units/mL of penicillin and 100 units/mL streptomycin, and cultured in a humidified 5% CO<sub>2</sub> incubator at 37°C. The  $\beta$ -gal activity of *lacZ*-transfected tumor cells was measured using a  $\beta$ -Gal Assay Kit with *o*-nitrophenyl- $\beta$ -*D*-galactopyranoside (Promega, Madison, WI, United States) and confirmed by X-gal or S-gal staining. Cells were fixed in PBS plus 0.5% glutaraldehyde (5 min) and rinsed in PBS prior to staining. Staining was performed using standard procedures for 2 h at 37°C in PBS plus 1 mg/ml X-gal (Sigma, St. Louis, MO, United States), 1 mM MgCl<sub>2</sub>, 5 mM K<sub>3</sub>Fe(CN)<sub>6</sub>, and 5 mM K<sub>4</sub>Fe(CN)<sub>6</sub> or with 1.5 mg/ml S-gal (Sigma, St. Louis, MO, United States) and 2.5 mg/ml FAC.

## Western Blot

The protein extracted from the wild-type and *lacZ*-expressing MCF7 and PC3 cancer cells was quantified using the Bradford method by a protein assay (Bio-Rad, Hercules, CA, United States). Protein (30  $\mu$ g) was added to each well, separated by 10% sodium dodecyl sulfate-polyacrylamide gel electrophoresis, and transferred to a polyvinylidene fluoride membrane. A primary monoclonal anti- $\beta$ -gal antibody (Promega, Madison, WI, United States) and anti-actin antibody (Sigma, St. Louis, MO, United States) were used as probes at a dilution of 1:5,000, with the reacting protein detected using a horseradish peroxidase-conjugated secondary antibody and ECL detection (Amersham, Piscataway, NJ, United States).

## Cytotoxicity

The cytotoxicity for the free  $\beta$ -D-galactopyranoside **AZ-1** and the released aglycone alizarine was assessed in both wild-type and *lacZ*-expressing MCF7 and PC3 cells using a colorimetric CellTiter 96 Aqueous Non-Radioactive Cell Proliferation Assay (MTS) (Promega, Madison, WI, United States). Assays were performed in triplicate using 24-well plates seeded with  $10^3$  cells per well in 500  $\mu$ L of RPMI-1640 without phenol red and supplemented with 10% FCS and 2 mM glutamine (Urano et al., 2005; Kamiya et al., 2007).

## DATA AVAILABILITY STATEMENT

The datasets presented in this study can be found in online repositories. The names of the repository/repositories and

accession number(s) can be found in the article/**Supplementary Material**.

## AUTHOR CONTRIBUTIONS

J-XY: conceived and designed the study, analyzed the data, and wrote the manuscript. SG, LZ, and ZF: synthesized, purified the compounds, and performed most part of NMR experiments. VK: conducted  $^1\text{H}$ -MRI experiments with PC3-*lacZ* cells and demonstrated the feasibility for detection of the *lacZ* gene expression. LL: conducted *lacZ* transfection in tumor cells and validated the  $\beta$ -gal activity. HW: assisted in toxicity evaluation. HX: helped with structural characterization. MT, BH, CC, and ZZ: assisted in processing data.

## FUNDING

This research was supported in part by the Research/Development Grants (2016QDJZR01 and HBMUPI201808) from the Biomedical Research Institute, fifth School of Medicine/Suizhou Central Hospital, Hubei University of Medicine, and the Natural Science Foundation of China (21877028).

## SUPPLEMENTARY MATERIAL

The Supplementary Material for this article can be found online at: <https://www.frontiersin.org/articles/10.3389/fchem.2021.709581/full#supplementary-material>

## REFERENCES

- Alam, J., and Cook, J. L. (1990). Reporter Genes: Application to the Study of Mammalian Gene Transcription. *Anal. Biochem.* 188, 245–254. doi:10.1016/0003-2697(90)90601-5
- Arena, F., Singh, J. B., Gianolio, E., Stefania, R., and Aime, S. (2011).  $\beta$ -Gal Gene Expression MRI Reporter in Melanoma Tumor Cells. Design, Synthesis, Andin Vitro and In Vivo Testing of a Gd(III) Containing Probe Forming a High Relaxivity, Melanin-like Structure upon  $\beta$ -Gal Enzymatic Activation. *Bioconjug. Chem.* 22, 2625–2635. doi:10.1021/bc200486j
- Asanuma, D., Sakabe, M., Kamiya, M., Yamamoto, K., Hiratake, J., Ogawa, M., et al. (2015). Sensitive  $\beta$ -galactosidase-targeting Fluorescence Probe for Visualizing Small Peritoneal Metastatic Tumours In Vivo. *Nat. Commun.* 6, 6463–6470. doi:10.1038/ncomms7463
- Bengtsson, N. E., Brown, G., Scott, E. W., and Walter, G. A. (2010). *LacZ* as a Genetic Reporter for Real-Time MRI. *Magn. Reson. Med.* 63, 745–753. doi:10.1002/mrm.22235
- Bertozi, C. R., and Kiessling, L. L. (2001). Chemical Glycobiology. *Science* 291, 2357–2364. doi:10.1126/science.1059820
- Beutler, E. (2004). CELL BIOLOGY: "Pumping" Iron: The Proteins. *Science* 306, 2051–2053. doi:10.1126/science.1107224
- Broome, A.-M., Ramamurthy, G., Lavik, K., Liggett, A., Kinstlinger, I., and Basilion, J. (2015). Optical Imaging of Targeted  $\beta$ -Galactosidase in Brain Tumors to Detect EGFR Levels. *Bioconjug. Chem.* 26, 660–668. doi:10.1021/bc500597y
- Browne, N. K., Huang, Z., Dockrell, M., Hashmi, P., and Price, R. G. (2010). Evaluation of New Chromogenic Substrates for the Detection of Coliforms. *J. Appl. Microbiol.* 108, 1828–1838. doi:10.1111/j.1365-2672.2009.04588.x
- Burke, H. M., Gunnlaugsson, T., and Scanlan, E. M. (2015). Recent Advances in the Development of Synthetic Chemical Probes for Glycosidase Enzymes. *Chem. Commun.* 51, 10576–10588. doi:10.1039/c5cc02793d
- Buss, J., Torti, F., and Torti, S. (2003). The Role of Iron Chelation in Cancer Therapy. *Cmc* 10, 1021–1034. doi:10.2174/0929867033457638
- Celen, S., Deroose, C., Groot, T. d., Chitneni, S. K., Gijssbers, R., Debyser, Z., et al. (2008). Synthesis and Evaluation of  $^{18}\text{F}$ - and  $^{11}\text{C}$ -Labeled Phenyl-Galactopyranosides as Potential Probes for In Vivo Visualization of LacZ Gene Expression Using Positron Emission Tomography. *Bioconjug. Chem.* 19, 441–449. doi:10.1021/bc700216d
- Chang, Y.-T., Cheng, C.-M., Su, Y.-Z., Lee, W.-T., Hsu, J.-S., Liu, G.-C., et al. (2007). Synthesis and Characterization of a New Bioactivated Paramagnetic Gadolinium(III) Complex [Gd(DOTA-FPG)(H<sub>2</sub>O)] for Tracing Gene Expression. *Bioconjug. Chem.* 18, 1716–1727. doi:10.1021/bc070019s
- Chatterjee, S. K., Bhattacharya, M., and Barlow, J. J. (1979). Glycosyltransferase and Glycosidase Activities in Ovarian Cancer Patients. *Cancer Res.* 39, 1943–1951.
- Chen, J., Jackson, A. A., Rotello, V. M., and Nugen, S. R. (2016). Colorimetric Detection of *Escherichia coli* Based on the Enzyme-Induced Metallization of Gold Nanorods Based on the Enzyme-Induced Metallization of Gold Nanorods. *Small* 12, 2469–2475. doi:10.1002/sml.201503682
- Chen, X., Ma, X., Zhang, Y., Gao, G., Liu, J., Zhang, X., et al. (2018). Ratiometric Fluorescent Probes with a Self-Immolative Spacer for Real-Time Detection of  $\beta$ -galactosidase and Imaging in Living Cells. *Analytica Chim. Acta* 1033, 193–198. doi:10.1016/j.aca.2018.05.071
- Chen, X., Zhang, X., Ma, X., Zhang, Y., Gao, G., Liu, J., et al. (2019). Novel Fluorescent Probe for Rapid and Ratiometric Detection of  $\beta$ -galactosidase and Live Cell Imaging. *Talanta* 192, 308–313. doi:10.1016/j.talanta.2018.09.061
- Coskuner, O., and Gonzalez, C. A. (2011). in *Metallic Systems: A Quantum Chemists Perspective, Chapter 3, Carbohydrate and Trivalent Iron Ion*

- Interactions*. Editors T. C. Allison and O. Coskuner (Gonzalez CA: CRC Press, Taylor & Francis Group), 83–106. 1420060775. 9781420060775.
- Cui, W., Liu, L., Kodibagkar, V. D., and Mason, R. P. (2010). S-Gal, A Novel  $^1\text{H}$  MRI Reporter for  $\beta$ -galactosidase. *Magn. Reson. Med.* 64, 66–71. doi:10.1002/mrm.22400
- Das, S., Bhattacharya, A., Mandal, P. C., Rath, M. C., and Mukherjee, T. (2002). One-electron Reduction of 1,2-Dihydroxy-9,10-Anthraquinone and Some of its Transition Metal Complexes in Aqueous Solution and in Aqueous Isopropanol-Acetone-Mixed Solvent: A Steady-State and Pulse Radiolysis Study. *Radiat. Phys. Chem.* 65, 93–100. doi:10.1016/s0969-806x(01)00451-0
- Das, S., Saha, A., and Mandal, P. C. (1995). Radiosensitization of Thymine by Fe(III)-1,2 Dihydroxyanthraquinone Complex in Dilute Aqueous Solution. *J. Radioanal. Nucl. Chem. Articles* 196, 57–63. doi:10.1007/bf02036289
- Davies, J. A., Dutremez, S. G., Hockensmith, C. M., Keck, R., Richardson, N., Selman, S., et al. (1996). Iron-based Second-Sphere Contrast Agents for Magnetic Resonance Imaging: Development of a Model System and Evaluation of Iron (III) Tris (Tironate) Complex in Rats. *Acad. Radiol.* 3, 936–945. doi:10.1016/s1076-6332(96)80305-9
- Dimri, G. P., Lee, X., Basile, G., Acosta, M., Scott, G., Roskelley, C., et al. (1995). A Biomarker that Identifies Senescent Human Cells in Culture and in Aging Skin *In Vivo*. *Proc. Natl. Acad. Sci.* 92, 9363–9367. doi:10.1073/pnas.92.20.9363
- Doura, T., Kamiya, M., Obata, F., Yamaguchi, Y., Hiyama, T. Y., Matsuda, T., et al. (2016). Detection of LacZ-Positive Cells in Living Tissue with Single-Cell Resolution. *Angew. Chem. Int. Ed.* 55, 9620–9624. doi:10.1002/anie.201603328
- Duo, T., Robinson, K., Greig, I. R., Chen, H.-M., Patrick, B. O., and Withers, S. G. (2017). Remarkable Reactivity Differences between Glucosides with Identical Leaving Groups. *J. Am. Chem. Soc.* 139, 15994–15999. doi:10.1021/jacs.7b09645
- Dwek, R. A. (1996). Glycobiology: Toward Understanding the Function of Sugars. *Chem. Rev.* 96, 683–720. doi:10.1021/cr940283b
- Espósito, F., Kharlamova, T., Distinto, S., Zinzula, L., Cheng, Y. C., Dutschman, G., et al. (2011). Alizarin Derivatives as New Dual Inhibitors of the HIV-1 Reverse Transcriptase-Associated DNA Polymerase and RNase H Activities Effective Also on the RNase H Activity of Non-nucleoside Resistant Reverse Transcriptases. *FEBS J.* 278, 1441–1457. doi:10.1111/j.1742-4658.2011.08057.x
- Feng, F., Liu, L., and Wang, S. (2009). Water-Soluble Conjugated Polyelectrolyte-Based Fluorescence Enzyme Coupling Protocol for Continuous and Sensitive  $\beta$ -Galactosidase Detection. *Macromol. Chem. Phys.* 210, 1188–1193. doi:10.1002/macp.200900264
- Fernández-Cuervo, G., Tucker, K. A., Malm, S. W., Jones, K. M., and Pagel, M. D. (2016). Diamagnetic Imaging Agents with a Modular Chemical Design for Quantitative Detection of  $\beta$ -Galactosidase and  $\beta$ -Glucuronidase Activities with CatalyCEST MRI. *Bioconjug. Chem.* 27, 2549–2557. doi:10.1021/acs.bioconjchem.6b00482
- Fernández-Tejada, A., Cañada, F. J., and Jiménez-Barbero, J. (2015). Recent Developments in Synthetic Carbohydrate-Based Diagnostics, Vaccines, and Therapeutics. *Chem. Eur. J.* 21, 10616–10628. doi:10.1002/chem.201500831
- Fu, W., Yan, C., Zhang, Y., Ma, Y., Guo, Z., and Zhu, W.-H. (2019). Near-Infrared Aggregation-Induced Emission-Active Probe Enables *In Situ* and Long-Term Tracking of Endogenous  $\beta$ -Galactosidase Activity. *Front. Chem.* 7, 291. doi:10.3389/fchem.2019.00291
- Gao, Z., Gao, H., Zheng, D., Xu, T., Chen, Y., Liang, C., et al. (2020).  $\beta$ -Galactosidase Responsive AIE Fluorogene for Identification and Removal of Senescent Cancer Cells. *Sci. China Chem.* 63, 398–403. doi:10.1007/s11426-019-9659-2
- Gorai, T., and Maitra, U. (2018). Eu/Tb Luminescence for Alkaline Phosphatase and  $\beta$ -galactosidase Assay in Hydrogels and on Paper Devices. *J. Mater. Chem. B* 6, 2143–2150. doi:10.1039/c7tb02657a
- Green, O., Gnaim, S., Blau, R., Eldar-Boock, A., Satchi-Fainaro, R., and Shabat, D. (2017). Near-Infrared Dioxetane Luminophores with Direct Chemiluminescence Emission Mode. *J. Am. Chem. Soc.* 139, 13243–13248. doi:10.1021/jacs.7b08446
- Gu, K., Qiu, W., Guo, Z., Yan, C., Zhu, S., Yao, D., et al. (2019). An Enzyme-Activatable Probe Liberating AIEgens: On-Site Sensing and Long-Term Tracking of  $\beta$ -galactosidase in Ovarian Cancer Cells. *Chem. Sci.* 10, 398–405. doi:10.1039/c8sc04266g
- Gu, K., Xu, Y., Li, H., Guo, Z., Zhu, S., Zhu, S., et al. (2016). Real-Time Tracking and *In Vivo* Visualization of  $\beta$ -Galactosidase Activity in Colorectal Tumor with a Ratiometric Near-Infrared Fluorescent Probe. *J. Am. Chem. Soc.* 138, 5334–5340. doi:10.1021/jacs.6b01705
- Gulaka, P. K., Yu, J.-X., Liu, L., Mason, R. P., and Kodibagkar, V. D. (2013). Novel S-Gal Analogs as  $^1\text{H}$  MRI Reporters for *In Vivo* Detection of  $\beta$ -galactosidase. *Magn. Reson. Imaging* 31, 1006–1011. doi:10.1016/j.mri.2013.03.001
- Haas, K. L., and Franz, K. J. (2009). Application of Metal Coordination Chemistry to Explore and Manipulate Cell Biology. *Chem. Rev.* 109, 4921–4960. doi:10.1021/cr900134a
- Haberhorn, U., Mier, W., and Eisenhut, M. (2005). Scintigraphic Imaging of Gene Expression and Gene Transfer. *Cmc* 12, 779–794. doi:10.2174/0929867053507351
- Han, J., Han, M. S., and Tung, C.-H. (2013). A Fluorogenic Probe for  $\beta$ -galactosidase Activity Imaging in Living Cells. *Mol. Biosyst.* 9, 3001–3008. doi:10.1039/c3mb70269c
- Hananya, N., and Shabat, D. (2019). Recent Advances and Challenges in Luminescent Imaging: Bright Outlook for Chemiluminescence of Dioxetanes in Water. *ACS Cent. Sci.* 5, 949–959. doi:10.1021/acscentsci.9b00372
- Hanaoka, K., Kikuchi, K., Terai, T., Komatsu, T., and Nagano, T. (2008). A  $\text{Gd}^{3+}$ -Based Magnetic Resonance Imaging Contrast Agent Sensitive to  $\beta$ -Galactosidase Activity Utilizing a Receptor-Induced Magnetization Enhancement (RIME) Phenomenon. *Chem. Eur. J.* 14, 987–995. doi:10.1002/chem.200700785
- Haris, M., Yadav, S. K., Rizwan, A., Singh, A., Wang, E., Hariharan, H., et al. (2015). Molecular Magnetic Resonance Imaging in Cancer. *J. Transl. Med.* 13, 313–329. doi:10.1186/s12967-015-0659-x
- Heffern, M. C., Matosziuk, L. M., and Meade, T. J. (2014). Lanthanide Probes for Bioresponsive Imaging. *Chem. Rev.* 114, 4496–4539. doi:10.1021/cr400477t
- Hingorani, D. V., Bernstein, A. S., and Pagel, M. D. (2015). A Review of Responsive MRI Contrast Agents: 2005–2014. *Contrast Media Mol. Imaging* 10, 245–265. doi:10.1002/cmim.1629
- Hu, J., Wu, Q., Cheng, K., Xie, Y., Li, C., and Li, Z. (2017). A  $^{19}\text{F}$  NMR Probe for the Detection of  $\beta$ -galactosidase: Simple Structure with Low Molecular Weight of 274.2, "Turn-On" Signal without the Background, and Good Performance Applicable in Cancer Cell Line. *J. Mater. Chem. B* 5, 4673–4678. doi:10.1039/c7tb00616k
- Hu, Q., Ma, K., Mei, Y., He, M., Kong, J., and Zhang, X. (2017). Metal-to-ligand Charge-Transfer: Applications to Visual Detection of  $\beta$ -galactosidase Activity and sandwich Immunoassay. *Talanta* 167, 253–259. doi:10.1016/j.talanta.2017.02.027
- Huang, J., Li, N., Wang, Q., Gu, Y., and Wang, P. (2017). A Lysosome-Targetable and Two-Photon Fluorescent Probe for Imaging Endogenous  $\beta$ -galactosidase in Living Ovarian Cancer Cells. *Sensors Actuators B: Chem.* 246, 833–839. doi:10.1016/j.snb.2017.02.158
- Huang, Y., Feng, H., Liu, W., Zhang, S., Tang, C., Chen, J., et al. (2017). Cation-driven Luminescent Self-Assembled Dots of Copper Nanoclusters with Aggregation-Induced Emission for  $\beta$ -galactosidase Activity Monitoring. *J. Mater. Chem. B* 5, 5120–5127. doi:10.1039/c7tb00901a
- Hudak, J. E., and Bertozzi, C. R. (2014). Glycotherapy: New Advances Inspire a Reemergence of Glycans in Medicine. *Chem. Biol.* 21, 16–37. doi:10.1016/j.chembiol.2013.09.010
- Ito, H., Kawamata, Y., Kamiya, M., Tsuda-Sakurai, K., Tanaka, S., Ueno, T., et al. (2018). Red-Shifted Fluorogenic Substrate for Detection of Lac Z-Positive Cells in Living Tissue with Single-Cell Resolution. *Angew. Chem. Int. Ed.* 57, 15702–15706. doi:10.1002/anie.201808670
- James, A. L., Perry, J. D., Chilvers, K., Robson, I. S., Armstrong, L., and Orr, K. E. (2000). Alizarin-beta-D-Galactoside: a New Substrate for the Detection of Bacterial Beta-Galactosidase. *Lett. Appl. Microbiol.* 30, 336–340. doi:10.1046/j.1472-765x.2000.00669.x
- Jiang, G., Zeng, G., Zhu, W., Li, Y., Dong, X., Zhang, G., et al. (2017). A Selective and Light-Up Fluorescent Probe for  $\beta$ -galactosidase Activity Detection and Imaging in Living Cells Based on an AIE Tetraphenylethylene Derivative. *Chem. Commun.* 53, 4505–4508. doi:10.1039/c7cc00249a
- Jiang, J., Tan, Q., Zhao, S., Song, H., Hu, L., and Xie, H. (2019). Late-stage Difluoromethylation Leading to a Self-Immobilizing Fluorogenic Probe for the Visualization of Enzyme Activities in Live Cells. *Chem. Commun.* 55, 15000–15003. doi:10.1039/c9cc07903c
- Josserand, V., Texier-Nogues, I., Huber, P., Favrot, M.-C., and Coll, J.-L. (2007). Non-invasive *In Vivo* Optical Imaging of the *lacZ* and *Luc* Gene Expression in Mice. *Gene Ther.* 14, 1587–1593. doi:10.1038/sj.gt.3303028
- Juers, D. H., Matthews, B. W., and Huber, R. E. (2012). LacZ $\beta$ -galactosidase: Structure and Function of an Enzyme of Historical and Molecular Biological Importance. *Protein Sci.* 21, 1792–1807. doi:10.1002/pro.2165

- Kamiya, M., Asanuma, D., Kuranaga, E., Takeishi, A., Sakabe, M., Miura, M., et al. (2011).  $\beta$ -Galactosidase Fluorescence Probe with Improved Cellular Accumulation Based on a Spirocyclized Rhodol Scaffold. *J. Am. Chem. Soc.* 133, 12960–12963. doi:10.1021/ja204781t
- Kamiya, M., Kobayashi, H., Hama, Y., Koyama, Y., Bernardo, M., Nagano, T., et al. (2007). An Enzymatically Activated Fluorescence Probe for Targeted Tumor Imaging. *J. Am. Chem. Soc.* 129, 3918–3929. doi:10.1021/ja067710a
- Kaplan, C. D., and Kaplan, J. (2009). Iron Acquisition and Transcriptional Regulation. *Chem. Rev.* 109, 4536–4552. doi:10.1021/cr9001676
- Kim, E.-J., Kumar, R., Sharma, A., Yoon, B., Kim, H. M., Lee, H., et al. (2017). *In Vivo* imaging of  $\beta$ -galactosidase Stimulated Activity in Hepatocellular Carcinoma Using Ligand-Targeted Fluorescent Probe. *Biomaterials* 122, 83–90. doi:10.1016/j.biomaterials.2017.01.009
- Kim, E.-J., Podder, A., Maiti, M., Lee, J. M., Chung, B. G., and Bhuniya, S. (2018). Selective Monitoring of Vascular Cell Senescence via  $\beta$ -Galactosidase Detection with a Fluorescent Chemosensor. *Sensors Actuators B: Chem.* 274, 194–200. doi:10.1016/j.snb.2018.07.171
- Kodibagkar, V. D., Yu, J., Liu, L., Hetherington, H. P., and Mason, R. P. (2006). Imaging  $\beta$ -galactosidase Activity Using  $^{19}\text{F}$  Chemical Shift Imaging of LacZ Gene-Reporter Molecule 2-Fluoro-4-Nitrophenol- $\beta$ -D-Galactopyranoside. *Magn. Reson. Imaging* 24, 959–962. doi:10.1016/j.mri.2006.04.003
- Koide, Y., Urano, Y., Yatsushige, A., Hanaoka, K., Terai, T., and Nagano, T. (2009). Design and Development of Enzymatically Activatable Photosensitizer Based on Unique Characteristics of Thiazole orange. *J. Am. Chem. Soc.* 131, 6058–6059. doi:10.1021/ja900443b
- Kong, X., Li, M., Dong, B., Yin, Y., Song, W., and Lin, W. (2019). An Ultrasensitivity Fluorescent Probe Based on the ICT-FRET Dual Mechanisms for Imaging  $\beta$ -Galactosidase *In Vitro* and *Ex Vivo*. *Anal. Chem.* 91, 15591–15598. doi:10.1021/acs.analchem.9b03639
- Kruger, A., Schirmacher, V., and Khokha, R. (1999). The Bacterial *lacZ* Gene: An Important Tool for Metastasis Research and Evaluation of New Cancer Therapies. *Cancer Metastasis Rev.* 17, 285–294.
- Kuznik, N., and Wyszocka, M. (2016). Iron(III) Contrast Agent Candidates for MRI: A Survey of the Structure-Effect Relationship in the Last 15 Years of Studies. *Eur. J. Inorg. Chem.*, 445–458. doi:10.1002/ejic.201501166
- Lee, H. W., Heo, C. H., Sen, D., Byun, H.-O., Kwak, I. H., Yoon, G., et al. (2014). Ratiometric Two-Photon Fluorescent Probe for Quantitative Detection of  $\beta$ -Galactosidase Activity in Senescent Cells. *Anal. Chem.* 86, 10001–10005. doi:10.1021/ac5031013
- Lee, H. W., Lim, C. S., Choi, H., Cho, M. K., Noh, C.-K., Lee, K., et al. (2019). Discrimination between Human Colorectal Neoplasms with a Dual-Recognitive Two-Photon Probe. *Anal. Chem.* 91, 14705–14711. doi:10.1021/acs.analchem.9b03951
- Li, H., and Meade, T. J. (2019). Molecular Magnetic Resonance Imaging with Gd(III)-based Contrast Agents: Challenges and Key Advances. *J. Am. Chem. Soc.* 141, 17025–17041. doi:10.1021/jacs.9b09149
- Li, X., Pan, Y., Chen, H., Duan, Y., Zhou, S., Wu, W., et al. (2020a). Specific Near-Infrared Probe for Ultrafast Imaging of Lysosomal  $\beta$ -Galactosidase in Ovarian Cancer Cells. *Anal. Chem.* 92, 5772–5779. doi:10.1021/acs.analchem.9b05121
- Li, X., Qiu, W., Li, J., Chen, X., Hu, Y., Gao, Y., et al. (2020b). First-generation Species-Selective Chemical Probes for Fluorescence Imaging of Human Senescence-Associated  $\beta$ -galactosidase. *Chem. Sci.* 11, 7292–7301. doi:10.1039/d0sc01234c
- Li, X., Zhang, Z., Yu, Z., Magnusson, J., and Yu, J.-X. (2013). Novel Molecular Platform Integrated Iron Chelation Therapy for  $^1\text{H}$ -MRI Detection of  $\beta$ -Galactosidase Activity. *Mol. Pharmaceutics* 10, 1360–1367. doi:10.1021/mp300627t
- Li, Y., Ning, L., Yuan, F., Zhang, T., Zhang, J., Xu, Z., et al. (2020). Activatable Formation of Emissive Excimers for Highly Selective Detection of  $\beta$ -Galactosidase. *Anal. Chem.* 92, 5733–5740. doi:10.1021/acs.analchem.9b04806
- Li, Z., Ren, M., Wang, L., Dai, L., and Lin, W. (2020). Development of a Red-Emissive Two-Photon Fluorescent Probe for Sensitive Detection of Beta-Galactosidase *In Vitro* and *In Vivo*. *Sensors Actuators B: Chem.* 307, 127643. doi:10.1016/j.snb.2019.127643
- Lilley, L. M., Kamper, S., Caldwell, M., Chia, Z. K., Ballweg, D., Vistain, L., et al. (2020). Self-Immulative Activation of  $\beta$ -Galactosidase-Responsive Probes for *In Vivo* MR Imaging in Mouse Models. *Angew. Chem. Int. Ed.* 59, 388–394. doi:10.1002/anie.201909933
- Liu, H.-W., Chen, L., Xu, C., Li, Z., Zhang, H., Zhang, X.-B., et al. (2018). Recent Progresses in Small-Molecule Enzymatic Fluorescent Probes for Cancer Imaging. *Chem. Soc. Rev.* 47, 7140–7180. doi:10.1039/c7cs00862g
- Liu, L., Kodibagkar, V. D., Yu, J.-X., and Mason, R. P. (2007).  $^{19}\text{F}$ -NMR Detection of *lacZ* Gene Expression via the Enzymic Hydrolysis of 2-fluoro-4-nitrophenyl  $\beta$ -D-galactopyranoside *In Vivo* in PC3 Prostate Tumor Xenografts in the Mouse 1. *FASEB j.* 21, 2014–2019. doi:10.1096/fj.06-7366lsf
- Liu, L., and Mason, R. P. (2010). Imaging  $\beta$ -Galactosidase Activity in Human Tumor Xenografts and Transgenic Mice Using a Chemiluminescent Substrate. *PLoS ONE* 5, e12024–31. doi:10.1371/journal.pone.0012024
- Louie, A. Y., Hüber, M. M., Ahrens, E. T., Rothbächer, U., Moats, R., Jacobs, R. E., et al. (2000). *In Vivo* visualization of Gene Expression Using Magnetic Resonance Imaging. *Nat. Biotechnol.* 18, 321–325. doi:10.1038/73780
- Lown, J. W. (1993). Anthracycline and Anthraquinone Anticancer Agents: Current Status and Recent Developments. *Pharmacol. Ther.* 60, 185–214. doi:10.1016/0163-7258(93)90006-y
- Lozano-Torres, B., Estepa-Fernández, A., Rovira, M., Orzáez, M., Serrano, M., Martínez-Mañez, R., et al. (2019). The Chemistry of Senescence. *Nat. Rev. Chem.* 3, 426–441. doi:10.1038/s41570-019-0108-0
- Lozano-Torres, B., Galiana, I., Rovira, M., Garrido, E., Chaib, S., Bernardos, A., et al. (2017). An Off-On Two-Photon Fluorescent Probe for Tracking Cell Senescence *In Vivo*. *J. Am. Chem. Soc.* 139, 8808–8811. doi:10.1021/jacs.7b04985
- Mahal, A., Villinger, A., and Langer, P. (2011). Site-selective Arylation of Alizarin and Purpurin Based on Suzuki-Miyaura Cross-Coupling Reactions. *Eur. J. Org. Chem.* 2011, 2075–2087. doi:10.1002/ejoc.201001497
- Malik, E. M., and Müller, C. E. (2016). Anthraquinones as Pharmacological Tools and Drugs. *Med. Res. Rev.* 36, 705–748. doi:10.1002/med.21391
- Mizukami, S., Matsushita, H., Takikawa, R., Sugihara, F., Shirakawa, M., and Kikuchi, K. (2011).  $^{19}\text{F}$  MRI Detection of  $\beta$ -galactosidase Activity for Imaging of Gene Expression. *Chem. Sci.* 2, 1151–1155.
- Nakamura, Y., Mochida, A., Nagaya, T., Okuyama, S., Ogata, F., Choyke, P. L., et al. (2017). A Topically-Sprayable, Activatable Fluorescent and Retaining Probe, SPIDER- $\beta$ Gal for Detecting Cancer: Advantages of Anchoring to Cellular Proteins after Activation. *Oncotarget* 8, 39512–39521. doi:10.18632/oncotarget.17080
- Nowak, R., and Tarasiuk, J. (2012). Anthraquinone Antitumour Agents, Doxorubicin, Pirarubicin and Benzoperimidine BPI, Trigger Caspase-3/caspase-8-dependent Apoptosis of Leukaemia Sensitive HL60 and Resistant HL60/VINC and HL60/DOX Cells. *Anticancer Drugs* 23, 380–392. doi:10.1097/cad.0b013e32834f8ab4
- Oushiki, D., Kojima, H., Takahashi, Y., Komatsu, T., Terai, T., Hanaoka, K., et al. (2012). Near-infrared Fluorescence Probes for Enzymes Based on Binding Affinity Modulation of Squarylium Dye Scaffold. *Anal. Chem.* 84, 4404–4410. doi:10.1021/ac300061a
- Pacheco-Rivera, R., Fattel-Fazenda, S., Arellanes-Robledo, J., Silva-Olivares, A., Alemán-Lazarini, L., Rodríguez-Segura, M., et al. (2016). Double Staining of  $\beta$ -galactosidase with Fibrosis and Cancer Markers Reveals the Chronological Appearance of Senescence in Liver Carcinogenesis Induced by Diethylnitrosamine. *Toxicol. Lett.* 241, 19–31. doi:10.1016/j.toxlet.2015.11.011
- Pang, X., Li, Y., Zhou, Z., Lu, Q., Xie, R., Wu, C., et al. (2020). Visualization of Endogenous  $\beta$ -galactosidase Activity in Living Cells and Zebrafish with a Turn-On Near-Infrared Fluorescent Probe. *Talanta* 217, 121098. doi:10.1016/j.talanta.2020.121098
- Paradis, V., Youssef, N., Dargère, D., Bâ, N., Bonvoust, F., Deschatrette, J., et al. (2001). Replicative Senescence in normal Liver, Chronic Hepatitis C, and Hepatocellular Carcinomas. *Hum. Pathol.* 32, 327–332. doi:10.1053/hupa.2001.22747
- Peng, L., Gao, M., Cai, X., Zhang, R., Li, K., Feng, G., et al. (2015). A Fluorescent Light-Up Probe Based on AIE and ESIP Processes for  $\beta$ -galactosidase Activity Detection and Visualization in Living Cells. *J. Mater. Chem. B* 3, 9168–9172. doi:10.1039/c5tb01938a
- Qiu, W., Li, X., Shi, D., Li, X., Gao, Y., Li, J., et al. (2020). A Rapid-Response Near-Infrared Fluorescent Probe with a Large Stokes Shift for Senescence-Associated  $\beta$ -galactosidase Activity Detection and Imaging of Senescent Cells. *Dyes Pigm.* 182, 108657. doi:10.1016/j.dyepig.2020.108657
- Razgulín, A., Ma, N., and Rao, J. (2011). Strategies for *In Vivo* Imaging of Enzyme Activity: An Overview and Recent Advances. *Chem. Soc. Rev.* 40, 4186–4216. doi:10.1039/c1cs15035a

- Rempel, B. P., Price, E. W., and Phenix, C. P. (2017). Molecular Imaging of Hydrolytic Enzymes Using PET and SPECT. *Mol. Imaging* 16, 1536012117717852–30. doi:10.1177/1536012117717852
- Richardson, D. R. (2005). Molecular Mechanisms of Iron Uptake by Cells and the Use of Iron Chelators for the Treatment of Cancer. *Cmc* 12, 2711–2729. doi:10.2174/092986705774462996
- Richardson, N., Davies, J. A., and Radüchel, B. (1999). Iron(III)-based Contrast Agents for Magnetic Resonance Imaging. *Polyhedron* 18, 2457–2482. doi:10.1016/s0277-5387(99)00151-5
- Sakabe, M., Asanuma, D., Kamiya, M., Iwatate, R. J., Hanaoka, K., Terai, T., et al. (2013). Rational Design of Highly Sensitive Fluorescence Probes for Protease and Glycosidase Based on Precisely Controlled Spirocyclization. *J. Am. Chem. Soc.* 135, 409–414. doi:10.1021/ja309688m
- Schwert, D. D., Davies, J. A., and Richardson, N. (2002). Non-gadolinium-based MRI Contrast Agents. *Top. Curr. Chem.* 221, 165–199. doi:10.1007/3-540-45733-x\_6
- Schwert, D. D., Richardson, N., Ji, G., Radüchel, B., Ebert, W., Heffner, P. E., et al. (2005). Synthesis of Two 3,5-disubstituted Sulfonamide Catechol Ligands and Evaluation of Their Iron(III) Complexes for Use as MRI Contrast Agents. *J. Med. Chem.* 48, 7482–7485. doi:10.1021/jm0501984
- Sharma, S. K., and Leblanc, R. M. (2017). Biosensors Based on  $\beta$ -galactosidase Enzyme: Recent Advances and Perspectives. *Anal. Biochem.* 535, 1–11. doi:10.1016/j.ab.2017.07.019
- Shi, L., Yan, C., Ma, Y., Wang, T., Guo, Z., and Zhu, W.-H. (2019). In Vivo ratiometric Tracking of Endogenous  $\beta$ -galactosidase Activity Using an Activatable Near-Infrared Fluorescent Probe. *Chem. Commun.* 55, 12308–12311. doi:10.1039/c9cc06869d
- Singh, H., Tiwari, K., Tiwari, R., Pramanik, S. K., and Das, A. (2019). Small Molecule as Fluorescent Probes for Monitoring Intracellular Enzymatic Transformations. *Chem. Rev.* 119, 11718–11760. doi:10.1021/acs.chemrev.9b00379
- Tang, C., Zhou, J., Qian, Z., Ma, Y., Huang, Y., and Feng, H. (2017). A Universal Fluorometric Assay Strategy for Glycosidases Based on Functional Carbon Quantum Dots:  $\beta$ -galactosidase Activity Detection In Vitro and in Living Cells. *J. Mater. Chem. B* 5, 1971–1979. doi:10.1039/c6tb03361j
- Terreno, E., Castelli, D. D., Viale, A., and Aime, S. (2010). Challenges for Molecular Magnetic Resonance Imaging. *Chem. Rev.* 110, 3019–3042. doi:10.1021/cr100025t
- Theil, E. C., and Goss, D. J. (2009). Living with Iron (And Oxygen): Questions and Answers about Iron Homeostasis. *Chem. Rev.* 109, 4568–4579. doi:10.1021/cr900052g
- Tung, C.-H., Zeng, Q., Shah, K., Kim, D.-E., Schellingerhout, D., and Weissleder, R. (2004). In Vivo Imaging of  $\beta$ -Galactosidase Activity Using Far Red Fluorescent Switch. *Cancer Res.* 64, 1579–1583. doi:10.1158/0008-5472.can-03-3226
- Urano, Y., Kamiya, M., Kanda, K., Ueno, T., Hirose, K., and Nagano, T. (2005). Evolution of Fluorescein as a Platform for Finely Tunable Fluorescence Probes. *J. Am. Chem. Soc.* 127, 4888–4894. doi:10.1021/ja043919h
- Van Dort, M. E., Lee, K. C., Hamilton, C. A., Rebebtulla, A., and Ross, B. D. (2008). Radiosynthesis and Evaluation of 5-[<sup>125</sup>I]iodoindol-3-yl- $\beta$ -D-Galactopyranoside as a  $\beta$ -galactosidase Imaging Radioligand. *Mol. Imaging* 7, 187–197. doi:10.2310/7290.2008.00020
- Wahsner, J., Gale, E. M., Rodríguez-Rodríguez, A., and Caravan, P. (2019). Chemistry of MRI Contrast Agents: Current Challenges and New Frontiers. *Chem. Rev.* 119, 957–1057. doi:10.1021/acs.chemrev.8b00363
- Wang, W., Vellaisamy, K., Li, G., Wu, C., Ko, C.-N., Leung, C.-H., et al. (2017). Development of a Long-Lived Luminescence Probe for Visualizing  $\beta$ -Galactosidase in Ovarian Carcinoma Cells. *Anal. Chem.* 89, 11679–11684. doi:10.1021/acs.analchem.7b03114
- Wang, Y., Liu, J., Ma, X., Cui, C., Deenik, P. R., Henderson, P. K. P., et al. (2019). Real-time Imaging of Senescence in Tumors with DNA Damage. *Sci. Rep.* 9, 2102. doi:10.1038/s41598-019-38511-z
- Weber, K. A., Achenbach, L. A., and Coates, J. D. (2006). Microorganisms Pumping Iron: Anaerobic Microbial Iron Oxidation and Reduction. *Nat. Rev. Microbiol.* 4, 752–764. doi:10.1038/nrmicro1490
- Wehrman, T. S., von Degenfeld, G., Krutzik, P. O., Nolan, G. P., and Blau, H. M. (2006). Luminescent Imaging of  $\beta$ -galactosidase Activity in Living Subjects Using Sequential Reporter-Enzyme Luminescence. *Nat. Methods* 3, 295–301. doi:10.1038/nmeth868
- Wei, X., Wu, Q., Zhang, J., Zhang, Y., Guo, W., Chen, M., et al. (2017). Synthesis of Precipitating Chromogenic/fluorogenic  $\beta$ -glucosidase/ $\beta$ -galactosidase Substrates by a New Method and Their Application in the Visual Detection of Foodborne Pathogenic Bacteria. *Chem. Commun.* 53, 103–106. doi:10.1039/c6cc07522c
- Wu, C., Ni, Z., Li, P., Li, Y., Pang, X., Xie, R., et al. (2020). A Near-Infrared Fluorescent Probe for Monitoring and Imaging of  $\beta$ -galactosidase in Living Cells. *Talanta* 219, 121307. doi:10.1016/j.talanta.2020.121307
- Xu, Z., Liu, C., Zhao, S., Chen, S., and Zhao, Y. (2019). Molecular Sensors for NMR-Based Detection. *Chem. Rev.* 119, 195–230. doi:10.1021/acs.chemrev.8b00202
- Yang, C., Wang, Q., and Ding, W. (2019). Recent Progress in the Imaging Detection of Enzyme Activities in Vivo. *RSC Adv.* 9, 25285–25302. doi:10.1039/c9ra04508b
- Yang, W., Zhao, X., Zhang, J., Zhou, Y., Fan, S., Sheng, H., et al. (2018). Hydroxyphenylquinazolinone-based Turn-On Fluorescent Probe for  $\beta$ -galactosidase Activity Detection and Application in Living Cells. *Dyes Pigm.* 156, 100–107. doi:10.1016/j.dyepig.2018.04.003
- Yeung, K., Schmid, K. M., and Phillips, S. T. (2013). A Thermally-Stable Enzyme Detection Assay that Amplifies Signal Autonomously in Water without Assistance from Biological Reagents. *Chem. Commun.* 49, 394–396. doi:10.1039/c2cc36861g
- Yu, J.-X., Kodibagkar, V. D., Liu, L., Zhang, Z., Liu, L., Magnusson, J., et al. (2013). MRS/<sup>1</sup>H-MRI Dual-Function Probe for Detection of  $\beta$ -galactosidase Activity. *Chem. Sci.* 4, 2132–2142.
- Yu, J.-X., Gulaka, P. K., Liu, L., Kodibagkar, V. D., and Mason, R. P. (2012a). Novel Fe<sup>3+</sup>-Based <sup>1</sup>H MRI  $\beta$ -Galactosidase Reporter Molecules. *ChemPlusChem* 77, 370–378. doi:10.1002/cplu.201100072
- Yu, J.-x., Kodibagkar, V., Cui, W., Mason, R., and F (2005). <sup>19</sup>F: A Versatile Reporter for Non-invasive Physiology and Pharmacology Using Magnetic Resonance. *Cmc* 12, 819–848. doi:10.2174/0929867053507342
- Yu, J.-X., Kodibagkar, V. D., Hallac, R. R., Liu, L., and Mason, R. P. (2012b). Dual<sup>19</sup>F/<sup>1</sup>H MR Gene Reporter Molecules Forin VivoDetection of  $\beta$ -Galactosidase. *Bioconjug. Chem.* 23, 596–603. doi:10.1021/bc200647q
- Yu, J.-X., Kodibagkar, V. D., Liu, L., and Mason, R. P. (2008a). A<sup>19</sup>F-NMR Approach Using Reporter Molecule Pairs to Assess  $\beta$ -Galactosidase in Human Xenograft Tumors in Vivo. *NMR Biomed.* 21, 704–712. doi:10.1002/nbm.1244
- Yu, J., Liu, L., Kodibagkar, V. D., Cui, W., and Mason, R. P. (2006). Synthesis and Evaluation of Novel Enhanced Gene Reporter Molecules: Detection of  $\beta$ -galactosidase Activity Using <sup>19</sup>F NMR of Trifluoromethylated Aryl  $\beta$ -D-galactopyranosides. *Bioorg. Med. Chem.* 14, 326–333. doi:10.1016/j.bmc.2005.08.021
- Yu, J., and Mason, R. P. (2006). Synthesis and Characterization of Novel lacZ Gene Reporter Molecules: Detection of  $\beta$ -Galactosidase Activity by <sup>19</sup>F Nuclear Magnetic Resonance of Polyglycosylated Fluorinated Vitamin B6. *J. Med. Chem.* 49, 1991–1999. doi:10.1021/jm051049o
- Yu, J. X., Cui, W., Zhao, D., and Mason, R. P. (2008b). Non-invasive Physiology and Pharmacology Using <sup>19</sup>F Magnetic Resonance, *Fluorine & Health - Molecular Imaging, Biomedical Materials and Pharmaceuticals*. (Amsterdam, Netherlands: Elsevier), 197–276. doi:10.1016/b978-0-444-53086-8.00005-9
- Yu, Z., Zhao, J., Hua, Z., Wang, X., Wang, X., Wang, H., et al. (2017). Novel<sup>19</sup>F-MRS  $\beta$ -galactosidase Reporter Molecules Incorporated Nitrogen Mustard Analogues. *Chem. Biol. Drug Des.* 90, 719–729. doi:10.1111/cbdd.12992
- Zeng, Z., Mizukami, S., Fujita, K., and Kikuchi, K. (2015). An Enzyme-Responsive Metal-Enhanced Near-Infrared Fluorescence Sensor Based on Functionalized Gold Nanoparticles. *Chem. Sci.* 6, 4934–4939. doi:10.1039/c5sc01850a
- Zeng, Z., Mizukami, S., and Kikuchi, K. (2012). Simple and Real-Time Colorimetric Assay for Glycosidases Activity Using Functionalized Gold Nanoparticles and its Application for Inhibitor Screening. *Anal. Chem.* 84, 9089–9095. doi:10.1021/ac301677v
- Zhang, C., Wang, D., Zhang, L., Guo, J.-F., and Ren, A.-M. (2016). Theoretical Investigation and Design of Two-Photon Fluorescent Probes for Visualizing  $\beta$ -galactosidase Activity in Living Cells. *RSC Adv.* 6, 70960–70971. doi:10.1039/c6ra11712k
- Zhang, J., Chai, X., He, X.-P., Kim, H.-J., Yoon, J., and Tian, H. (2019a). Fluorogenic Probes for Disease-Relevant Enzymes. *Chem. Soc. Rev.* 48, 683–722. doi:10.1039/c7cs00907k

- Zhang, J., Cheng, P., and Pu, K. (2019b). Recent Advances of Molecular Optical Probes in Imaging of  $\beta$ -Galactosidase. *Bioconj. Chem.* 30, 2089–2101. doi:10.1021/acs.bioconjchem.9b00391
- Zhang, J., Li, C., Dutta, C., Fang, M., Zhang, S., Tiwari, A., et al. (2017). A Novel Near-Infrared Fluorescent Probe for Sensitive Detection of  $\beta$ -galactosidase in Living Cells. *Analytica Chim. Acta* 968, 97–104. doi:10.1016/j.aca.2017.02.039
- Zhang, X.-X., Wu, H., Li, P., Qu, Z.-J., Tan, M.-Q., and Han, K.-L. (2016). A Versatile Two-Photon Fluorescent Probe for Ratiometric Imaging *E. coli*  $\beta$ -galactosidase in Live Cells and *In Vivo*. *Chem. Commun.* 52, 8283–8286. doi:10.1039/c6cc04373a
- Zhang, X., Chen, X., Zhang, Y., Liu, K., Shen, H., Zheng, E., et al. (2019). A Near-Infrared Fluorescent Probe for the Ratiometric Detection and Living Cell Imaging of  $\beta$ -galactosidase. *Anal. Bioanal. Chem.* 411, 7957–7966. doi:10.1007/s00216-019-02181-7
- Zhao, X., Yang, W., Fan, S., Zhou, Y., Sheng, H., Cao, Y., et al. (2019). A Hemicyanine-Based Colorimetric Turn-On Fluorescent Probe for  $\beta$ -galactosidase Activity Detection and Application in Living Cells. *J. Lumin.* 205, 310–317. doi:10.1016/j.jlumin.2018.09.036
- Zhou, Z., Bai, R., Munasinghe, J., Shen, Z., Nie, L., and Chen, X. (2017). T1-T2 Dual-Modal Magnetic Resonance Imaging: From Molecular Basis to Contrast Agents. *ACS Nano* 11, 5227–5232. doi:10.1021/acsnano.7b03075
- Zhu, W. H., Chen, J. A., Pan, H., Wang, Z., Gao, J., Tan, J., et al. (2020). Imaging of Ovarian Cancers Using Enzyme Activatable Probes with Second Near-Infrared Window Emission. *Chem. Commun. (Camb)* 56, 2731–2734. doi:10.1039/c9cc09158k

**Conflict of Interest:** The authors declare that the research was conducted in the absence of any commercial or financial relationships that could be construed as a potential conflict of interest.

Copyright © 2021 Gao, Zhao, Fan, Kodibagkar, Liu, Wang, Xu, Tu, Hu, Cao, Zhang and Yu. This is an open-access article distributed under the terms of the Creative Commons Attribution License (CC BY). The use, distribution or reproduction in other forums is permitted, provided the original author(s) and the copyright owner(s) are credited and that the original publication in this journal is cited, in accordance with accepted academic practice. No use, distribution or reproduction is permitted which does not comply with these terms.